UNCERTAINTY ESTIMATION IN PRIMARY RADIOMETRIC TEMPERATURE MEASUREMENT

JULY 2018

Peter Saunders[1], Emma Woolliams[2], Howard Yoon[3], Andrew Todd[4], Mohamed Sadli[5],

Eric van der Ham[6], Klaus Anhalt[7], Lutz Werner[7], Dieter R. Taubert[7],

Stephan Briaudeau[5], Boris Khlevnoy[8]

[1]MSL, Lower Hutt, New Zealand
[2]NPL, Teddington, United Kingdom
[3]NIST, Gaithersburg, United States of America
[4]NRC, Ottawa, Canada
[5]LNE-CNAM, St Denis, France
[6]NMIA, Sydney, Australia
[7]PTB, Berlin, Germany
[8]VNIIOFI, Moscow, Russian Federation

Table of Contents

1. Scope

The *mise-en-pratique* for the definition of the kelvin describes *absolute primary radiometric thermometry* as an approach for thermodynamic temperature measurement based on an accurate determination of the optical power emitted, over a known spectral band and known solid angle, by an isothermal cavity of known emissivity. This report has been produced by members of the CCT Working Group on Non-Contact Thermometry (CCT-WG-NCTh) to describe the methods used for determining the uncertainty associated with thermodynamic temperature as measured using absolute primary radiometric thermometry. The uncertainty components given in the report are described as "best" and "normal", where best uncertainties are those that can be obtained with considerable effort by a small number of leading workers in the field, and normal uncertainties are those that can easily be obtained at present in national metrology institutes. All uncertainties given in this document are standard uncertainties.

2. Radiometric Measurement of Thermodynamic Temperature

2.1 Measurement of Radiance

The determination of thermodynamic temperature through filter radiometry involves the measurement of the spectral radiance of a blackbody source using an instrument known variously as a 'filter radiometer' or 'absolute radiation thermometer'. Such an instrument consists of a detector and spectral filter[1], and an optical system, typically including two co-aligned circular apertures that define the solid angle, and, optionally, additional lenses or mirrors.

The blackbody spectral radiance is given by Planck's law, which, for measurements where the detector is in air, is

$$L_b(\lambda, T) = \left(\frac{2hc^2}{n^2\lambda^5} \right) \frac{1}{\exp\left[hc/(n\lambda kT) \right] - 1}, \tag{1}$$

where T is the thermodynamic temperature, k is the Boltzmann constant, h is the Planck constant, c is the speed of light in a vacuum, n is the refractive index of the air [1, 2] at the detector, and λ is the wavelength in air. The constants in Eq. (1) are usually written in terms of the first and second radiation constants, $c_1 = 2hc^2 = 1.191\,042\,972 \times 10^{-16}\ \mathrm{W\,m^2}$ and $c_2 = hc/k = 0.014\,387\,768\ \mathrm{m\,K}$.

The temperature of the blackbody is determined by measuring the spectral radiance within a defined spectral band. The units of spectral radiance are $\mathrm{W\,m^{-2}\,sr^{-1}\,nm^{-1}}$ and, therefore, a primary radiometric determination of thermodynamic temperature requires the power measurement to be traceable to the definition of the watt, and wavelength, area, and distance measurements to the definition of the metre. Generally, this is achieved as follows:

- **Power:** via a responsivity calibration of the filter radiometer against a trap detector that has been calibrated against a cryogenic radiometer.
- **Wavelength:** by making the responsivity calibration at discrete wavelengths using a calibrated tuneable monochromatic source. This is often achieved using a tuneable laser illuminating an integrating sphere [3, 4] or, alternatively, a monochromator-based source [5, 6]. The wavelength determination of the laser, or the wavelength scale calibration of the monochromator using atomic emission lines [7], provides traceability to the metre.
- **Area and distance:** via two precision circular apertures with known diameters and separation.

2.2 The Geometric Factor (Form Factor, Configuration Factor)

Consider the simple case of a coaxial system consisting of a blackbody, two apertures, and a detector. The blackbody is a Lambertian source and, therefore, the flux, Φ, that leaves the first aperture and radiates into the full hemisphere is determined by the area, A_1, of the first aperture and the radiance of the blackbody:

$$\Phi_{A_1} = A_1 \pi L_b. \tag{2}$$

---

[1] Which may be a glass or interference filter, or may be created using an instrument such as a monochromator.

The form factor is the fraction of radiation emitted by one Lambertian surface that is intercepted directly by a second surface. The form factor for two coaxial parallel circular apertures of radii r_1 and r_2 and separation d is:

$$F_{A_1-A_2} = \frac{2r_2^2}{(r_1^2 + r_2^2 + d^2) + \sqrt{(r_1^2 + r_2^2 + d^2)^2 - 4r_1^2 r_2^2}} \; . \tag{3}$$

The flux that reaches the second aperture is equal to the flux emitted by the first aperture multiplied by the form factor; i.e.,

$$\Phi_{A_2} = A_1 \pi L_b F_{A_1-A_2} . \tag{4}$$

It is sometimes helpful to introduce a geometric factor, g, defined as

$$g = A_1 F_{A_1-A_2} = \frac{2\pi r_1^2 r_2^2}{(r_1^2 + r_2^2 + d^2) + \sqrt{(r_1^2 + r_2^2 + d^2)^2 - 4r_1^2 r_2^2}} \; , \tag{5}$$

so that the flux is calculated from

$$\Phi_{A_2} = g \pi L_b . \tag{6}$$

The geometric factor is symmetrical with respect to the two apertures, so distinguishing between a 'first' and a 'second' aperture is not required.

2.3 Four Calibration Schemes

As currently realised, filter radiometers comprise a detector, a spectrally-selective filter, and a geometric/optical system with two defining apertures. For illustrative purposes, four different implementations are described below (and in the *mise en pratique*), each having a slightly different calibration method.

- A filter radiometer, calibrated for power responsivity, used to measure the radiance of the blackbody in combination with detector and source apertures – the *spectral power method*.
- A filter radiometer, calibrated for irradiance responsivity, used to measure the radiance of the blackbody in combination with a source aperture – the *irradiance method*.
- A filter radiometer, calibrated for irradiance responsivity, used to measure the radiance of the blackbody in combination with a lens aperture and a single, simple lens – the *hybrid method*.
- An imaging radiometer, calibrated for radiance responsivity, comprising a filter radiometer incorporated within an optical system consisting of several lenses and appropriate baffling – the *radiance method*.

The first two methods are non-imaging and the second two use optics to facilitate the measurement of small sources.

2.4 The Basic Measurement Equation

Whichever scheme is used, the measurement equation takes the form

$$i = \int_0^\infty s_L(\lambda) L_b(\lambda, T) d\lambda \,, \tag{7}$$

where i is the measured photocurrent, $s_L(\lambda)$ is the spectral radiance responsivity [units: A W^{-1} m^2 sr] of the combined instrument, $L_b(\lambda, T)$ is the spectral radiance of the blackbody, as given by Eq. (1), λ is the wavelength in air, and T is the thermodynamic temperature. This expression will be modified somewhat for the different schemes.

For the *spectral power method*, the radiometer is calibrated for flux responsivity [units: A W^{-1}] and two apertures are added for the blackbody measurement (see Figure 1). Equation (7) is implemented using

$$\text{Spectral power:} \qquad s_L(\lambda) = \pi g s_\Phi(\lambda)\,, \tag{8}$$

where g is the geometric factor for the added double aperture system, given by Eq. (5), and $s_\Phi(\lambda)$ is the spectral flux responsivity of the filter radiometer.

a) Calibration   b) Use
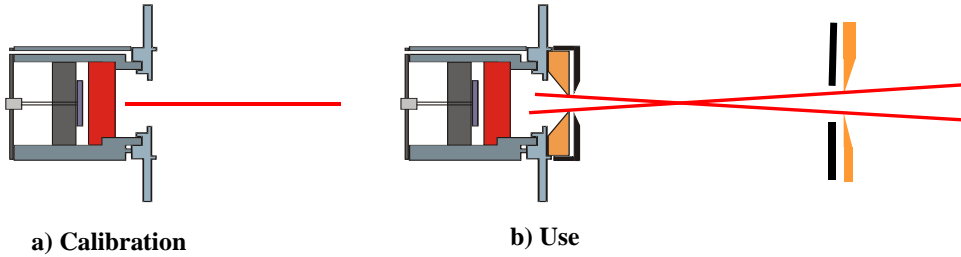
Figure 1. The power method.

For the *irradiance method*, the radiometer is calibrated for irradiance responsivity [units: A W^{-1} m^2] with an overfilled aperture. It is then used with a second aperture added for the blackbody measurement (see Figure 2). Equation (7) is implemented using

$$\text{Irradiance:} \qquad s_L(\lambda) = \frac{\pi g s_E(\lambda)}{A_{FR}}\,, \tag{9}$$

where g is the geometric factor for the double aperture system, given by Eq. (5), after the second aperture is added, A_{FR} is the filter radiometer's aperture area, and $s_E(\lambda)$ is the irradiance responsivity of the filter radiometer.

a) Calibration   **b) Use**
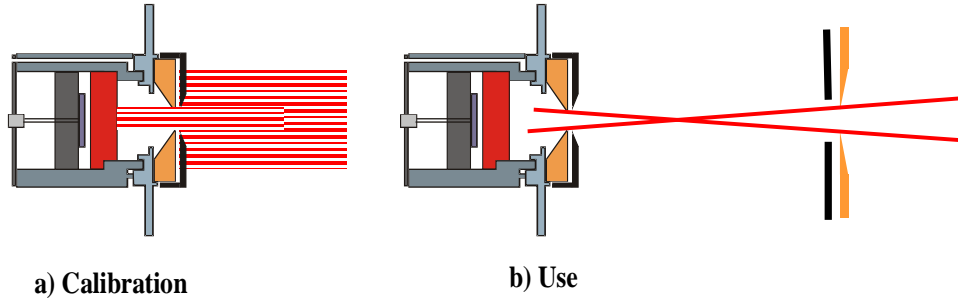
Figure 2. The irradiance method.

For the *hybrid method*, the setup is similar to the irradiance method, but an additional lens is introduced to enable the measurement of smaller sources (see Figure 3). Here, Eq. (7) is implemented using

$$\text{Hybrid:} \qquad s_L(\lambda) = \frac{\pi g s_E(\lambda)\tau(\lambda)}{A_{\text{FR}}}, \qquad (10)$$

where g is the geometric factor for the double aperture system, given by Eq. (5), after the second aperture is added, A_{FR} is the filter radiometer's aperture area, $s_E(\lambda)$ is the irradiance responsivity of the filter radiometer, and $\tau(\lambda)$ is the spectral transmittance of the lens.

a) Calibration   **b) Use**
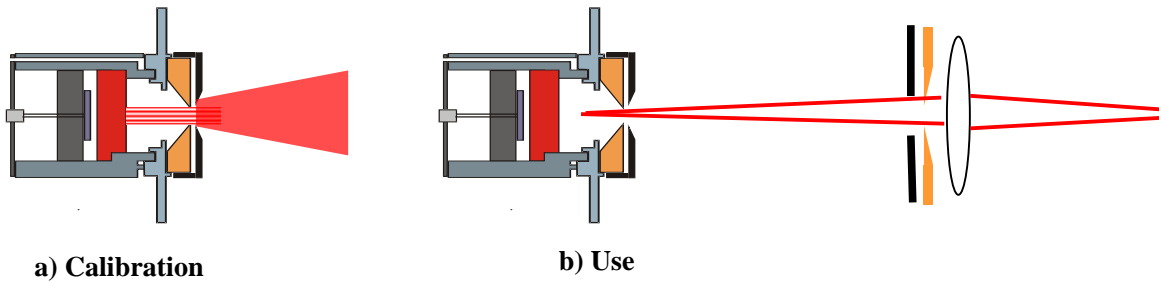
Figure 3. The hybrid method.

For the *radiance method*, Eq. (7) can be used directly, as here the instrument is calibrated for radiance responsivity (see Figure 4).
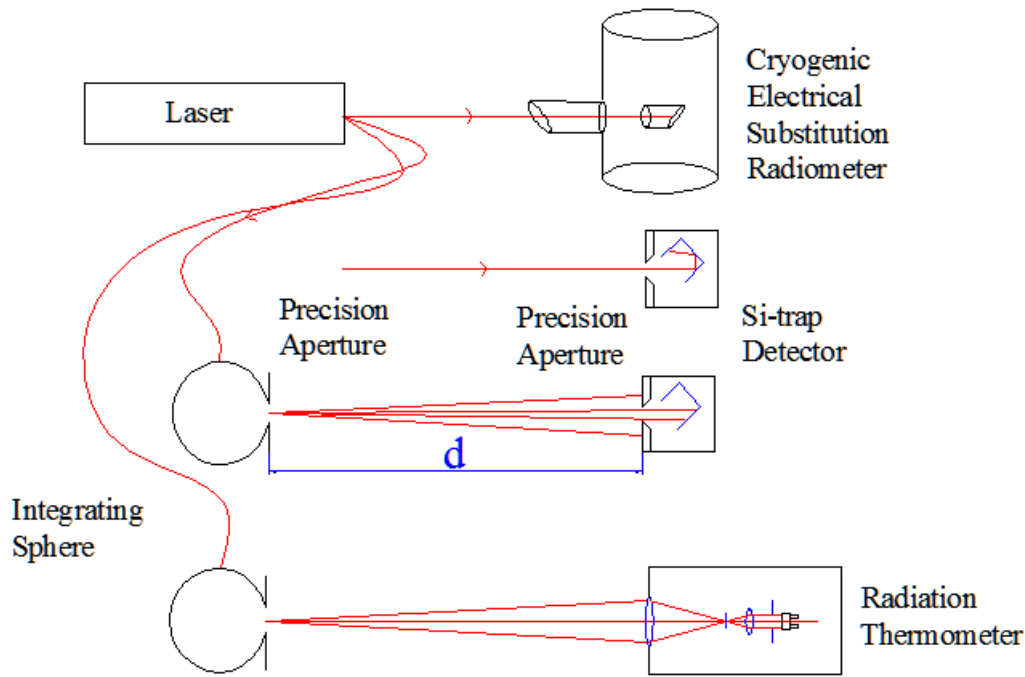
Figure 4. The radiance method.

2.5 The Generic Measurement Equation

Generally, Eq. (7) has additional multiplying constants to account for various corrections. The measured signal may be, for example, a voltage

$$V_{\text{signal}} = i \times G_{\text{amp}}, \tag{11}$$

where G_{amp} is the gain of a transimpedance amplifier [units: V A^{-1}].

There will be further corrections for other effects. The hybrid and radiance methods will have a size-of-source effect (SSE) correction due to lens scatter (see Sections 6.1.1 and 6.1.2). The irradiance and power methods will have a similar diffraction correction for diffraction at the first aperture (see Section 4.1.7). These provide an additional correction factor, here generically given by the symbol K_{SSE}. The power, irradiance, and hybrid methods will also have a correction for stray light, K_{stray} (see Section 4.1.6).

There may be a correction for blackbody emissivity, ε_{BB}, which is generally considered to be a constant over the spectral responsivity of the filter radiometer (but may need to be treated as a spectral quantity for wide bandwidths). There may also be a correction for instrument linearity between the calibration and blackbody signal levels, K_{lin} (see Section 6.1.3), and a correction for out-of-band transmittance, K_{OOB} (see Section 4.1.5). Thus, for example, for the hybrid method Eq. (7) may be written

$$V_{\text{signal}} = \frac{\pi g}{A_{\text{FR}}} \varepsilon_{\text{BB}} G_{\text{amp}} K_{\text{OOB}} K_{\text{stray}} K_{\text{SSE}} K_{\text{lin}} \int_0^\infty s_E(\lambda)\tau(\lambda)L_{\text{b}}(\lambda,T)d\lambda \ . \qquad (12)$$

For the purposes of uncertainty analysis, it is helpful to write this in a generic way to simplify the mathematical expressions. Therefore, for the mathematical sections of this report, we use a generic version of this expression. Note that later sections describe how to interpret this generic notation for specific cases. Thus, the generic version of the equation is:

$$\text{Generic:} \qquad S = K \int_0^\infty s(\lambda)L_{\text{b}}(\lambda,T)d\lambda \ , \qquad (13)$$

where S is the measured temperature-dependent "signal", which may be in amps, volts, or digital numbers, depending on the device, $s(\lambda)$ is the radiance, irradiance, or power responsivity of the filter radiometer, as appropriate (and for the hybrid case also includes the lens transmittance), K includes all the optical, geometrical, and electrical quantities not included in $s(\lambda)$, and $L_{\text{b}}(\lambda,T)$ is the blackbody spectral radiance.

2.6 Determining the Temperature of the Blackbody

Generally, Eq. (13), with the appropriate corrections (e.g., in the form of Eq. (12)), is solved numerically by iteratively varying T until the calculated signal (the right-hand side of Eq. (13)) is equal to the measured signal, S. Methods such as the bisection rule can be used to achieve this, but the most efficient method is to use the Newton-Raphson algorithm, based on an initial estimate T_0. The algorithm then proceeds by forming successively better estimates, T_i, for $i = 1, 2, 3, \ldots$, using the formula

$$T_{i+1} = T_i + \frac{S - K \int_0^\infty s(\lambda)L_{\text{b}}(\lambda,T_i)d\lambda}{\dfrac{c_2}{T_i^2} K \int_0^\infty s(\lambda)\dfrac{L_{\text{b}}(\lambda,T_i)}{n\lambda\left[1-\exp\left(-c_2/(n\lambda T_i)\right)\right]}d\lambda} \ . \qquad (14)$$

Convergence to better than 0.1 mK is usually achieved in fewer than 5–10 iterations, depending on how close the initial guess, T_0, is to the true temperature [8].

3. Uncertainty Analysis

3.1 Categorising the Uncertainty Components

For the purposes of this report, the uncertainty components are separated into four categories, as shown in Figure 5. The main split is between those sources of uncertainty that are due to the calibration of the filter radiometer and those that are due to its use in measuring a blackbody. Some sources of uncertainty for the filter radiometer calibration are common to all four calibration schemes (Section 4.1), while others are specific to one scheme. The sources of uncertainty relating to the measurement of a blackbody can themselves be split into those due to the source and those due to the filter radiometer.
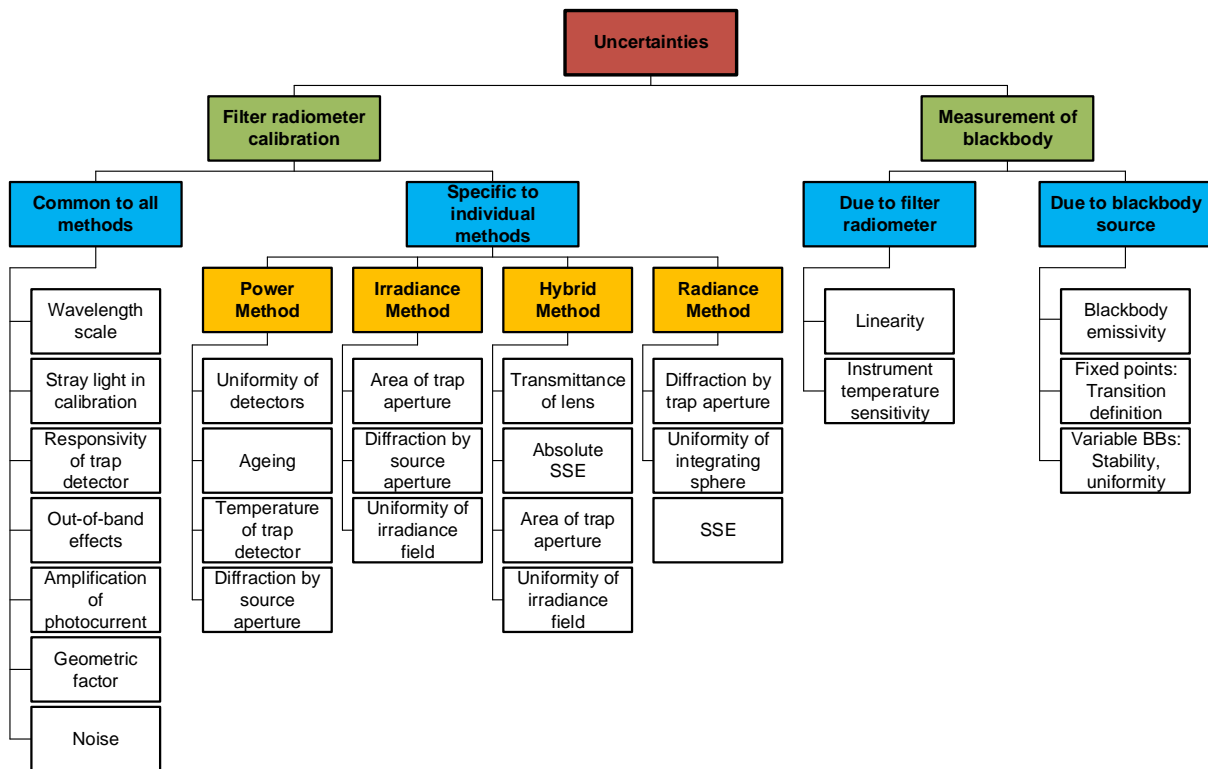
Figure 5. Classification of the uncertainty components.

3.2 Overview of Uncertainty Analysis

The measurement equation, written in generic notation as Eq. (13), relates the measured signal to the source temperature, T. Uncertainty associated with any of the factors or parameters in Eq. (13), determined either during the calibration phase or during use to determine an unknown temperature, must be propagated through this equation to calculate its influence on the calculated value of T. As the expression cannot be rearranged into the direct form $T = f(x_1, x_2, \ldots)$, the uncertainty analysis requires implicit differentiation. The sensitivity coefficient for any standard uncertainty component $u(x_i)$ can be determined from:

$$\frac{\partial T}{\partial x_i} = -\frac{\partial S}{\partial x_i} \Big/ \frac{\partial S}{\partial T} .\tag{15}$$

The total standard uncertainty associated with the calculated temperature is then, in accordance with the law of propagation of uncertainties [9],

$$u(T) = \left[\sum_i \left(\frac{\partial T}{\partial x_i} u(x_i) \right)^2 + \sum_i \sum_{j, j \neq i} \frac{\partial T}{\partial x_i} \frac{\partial T}{\partial x_j} r(x_i, x_j) u(x_i) u(x_j) \right]^{1/2} ,\tag{16}$$

where $r(x_i, x_j)$ is the correlation coefficient between the uncertainties $u(x_i)$ and $u(x_j)$.

There are two approaches to deriving these sensitivity coefficients. One method, described in Appendix A, is based on the full integral of Eq. (13). The second method, described in Appendix B, approximates the measurement equation by an analytic equation based on key spectral parameters of the filter radiometer, which can be used to calculate T directly.

3.3 Correlation

There are two ways in which correlation affects the uncertainty analysis:
- Where multiple measured values are combined, it is necessary to distinguish those sources of uncertainty that are systematic between the combined measurements (for example, if the same filter radiometer is used, then its calibration can be considered common) and those that change from one measurement to the next (for example, measurement noise).
- The measurement equation, Eq. (13), integrates the product of the Planck function and the spectral responsivity of the filter radiometer. The spectral responsivity of the filter radiometer is determined at discrete wavelength values by comparison with the trap detector. In order to estimate the uncertainty associated with the integrated quantity, it is necessary to understand the correlation between the measured values at the discrete wavelengths.

This section concentrates on the second condition – the implication of correlation on the spectral integral. It is also necessary to consider that there will be uncertainties associated with both the wavelength scale (horizontal axis in graphed spectral responsivity) and with the responsivity (vertical axis in graphed spectral responsivity), and for both wavelength and responsivity effects there are some sources of uncertainty that are fully correlated, some that are partially correlated, and some that are uncorrelated.

3.3.1 Uncertainties associated with wavelength

During the filter radiometer spectral calibration, the responsivity is determined at several wavelengths using a monochromatic, or pseudo-monochromatic, source created using either a tuneable laser or a monochromator illuminated by a broadband source. The calibration of the wavelength scale of a laser and monochromator is described in Section 4.1.4. Where a wavemeter is used with a laser, the uncertainties are generally small. The worst-case scenario would be when these uncertainties are fully uncorrelated.

A monochromator's wavelength scale is itself calibrated against reference wavelengths. Here there will be wavelength uncertainties in all three categories. The accuracy of the wavelength scale

calibration will be a fully correlated (systematic-wavelength) effect. The reproducibility of the wavelength scale (repeatability of the grating rotation) will be a fully uncorrelated (random-wavelength) effect. Any sine-bar error, which creates a reproducible spectral shape to the wavelength scale error, will be a partially-correlated effect.

3.3.2 Uncertainties associated with the spectral responsivity

Assuming that the calibration is performed in 'one go' (i.e., the filter radiometer is not realigned from one wavelength to the next), then all sources of uncertainty relating to the setup (e.g., alignment, geometry, diffraction) will be correlated effects, affecting the spectral responsivity equally at all wavelengths. Stray light and source non-uniformity are usually also spectrally 'flat' across the spectral range of a filter radiometer.

Measurement noise (whether electrical or optical) is always a random effect, and, assuming that the measurements take a considerable period of time, fluctuations in, for example, room temperature, as well as source stability, will also be uncorrelated (having a random effect on the responsivity values determined from one wavelength to the next).

Partial correlation will come from a slow drift during the measurements of, for example, the reference detector, from room temperature variations, or from a drift in the instrument alignment. Here, measured values at wavelengths taken closer together in time will have a higher correlation than those taken at, for example, the beginning and end of a scan. Partial correlation is also introduced through mathematical interpolations of the reference detector's spectral responsivity. If the filter radiometer is relatively narrowband, then the reference detector's spectral responsivity may be based on a single wavelength value and, therefore, the uncertainty associated with the reference detector's responsivity will create a fully correlated effect in the filter radiometer's spectral responsivity. On the other hand, if the filter radiometer is broadband, then the reference detector's responsivity will be based on several measured values, and in this case the effect will be partially correlated.

3.3.3 Application of correlation information

The application of correlation information is discussed in Appendices A and B. In these appendices, the wavelength uncertainties are separated into fully correlated components and fully uncorrelated components, and propagation of uncertainty formulae, based on Eq. (16), are explicitly derived for these two cases (i.e., when $r(\lambda_i, \lambda_j) = 1$ for all i and j, and when $r(\lambda_i, \lambda_j) = 1$ only when $i = j$ and is zero otherwise). Partially-correlated uncertainties are easily dealt with if the values of $r(\lambda_i, \lambda_j)$ are known, since all of the sensitivity coefficients in Eq. (16) are given. Propagation of uncertainty formulae for the spectral responsivity values are similarly derived.

4. Calibration of the Filter Radiometer

4.1 Common Sources of Uncertainty

This section describes sources of uncertainty that are common to all four of the calibration schemes discussed in Section 2.3. There may be some differences in how these uncertainties are assessed for each calibration scheme, and those differences are discussed in the relevant sections below (Section 4.2).

4.1.1 Power responsivity of a trap detector

The spectral power responsivity, $s_{\Phi,\mathrm{trap}}(\lambda)$, of a photodiode-based trap detector is defined as the ratio of the photocurrent, I, to the incident radiant power, P, causing the photocurrent:

$$s_{\Phi,\mathrm{trap}}(\lambda) = I/P. \tag{17}$$

The photocurrent measurement is usually performed by a current-to-voltage converter (Section 4.1.2) and a digital voltmeter. The radiant power is measured using a cryogenic radiometer, which is an electrical substitution radiometer operated at low temperatures, slightly above the boiling point of liquid helium. The radiation sources can be subdivided into three main types: (i) a monochromator in conjunction with a broadband radiation source (e.g., an argon arc plasma, a xenon arc, or a tungsten-halogen lamp); (ii) a widely and continuously wavelength-tuneable laser system; and (iii) a laser system delivering radiation at widely separated laser lines (e.g., a krypton ion laser). The first two systems allow, in principle, the determination of the spectral responsivity at any wavelength of interest. In practice, the measurements are performed at wavelengths separated by intervals ranging from about 2 nm to 20 nm. The last system (iii) is restricted to measurements at the available laser lines, which are usually widely separated. In all cases, the measured spectral responsivity must be interpolated over the entire wavelength range of interest using empirical or physical models. When the trap detector is applied to measure the radiant power in order to calibrate a filter radiometer, its spectral responsivity has to be corrected for the experimental conditions (e.g., radiant power, temperature, spot size, polarisation state, etc.) during the calibration of the filter radiometer, which usually strongly differ from those during the calibration of the trap detector.

The uncertainty contributions can be grouped as follows:
- G1. *Uncertainty of the radiant power measurement by the cryogenic radiometer.*
  These contributions mainly depend on the type of cryogenic radiometer used and the effort spent to characterise the device.
- G2. *Uncertainty contributions related to the trap detector calibration against the cryogenic radiometer.*
  These contributions mainly depend on the calibration principle, the radiation source, and the facility used to calibrate a trap detector against a cryogenic radiometer.
- G3. *Uncertainty contributions arising from the interpolation of the spectral responsivity.*
- G4. *Uncertainty contributions related to the use of the calibrated trap detector under experimental conditions different from those during its calibration.*
  These contributions depend on the properties of the filter radiometer to be calibrated and the degree of mismatch of the experimental conditions of the calibration and the use of the trap detector.

An example of an uncertainty budget is shown in the Table 1.

Table 1. Example uncertainty budget for the power responsivity of a trap detector.

Source of uncertainty	$10^6 \times$ relative standard uncertainty
G1 (radiant power measurement):	
Electrical power measurements	5
Non-equivalence of electrical/optical power	10
Cavity absorptance	10
Window transmittance	18
Sensitivity of the radiometer	10
Repeatability	15
Total uncertainty of group G1	**30**
G2 (Detector calibration):	
Stray radiation	20
Photocurrent	10
Wavelength	2
Distance and diameter effects	20
Total uncertainty of group G2	**30**
G3 (Interpolation/Fit):	
Interpolation/fit of the spectral responsivity	200
Total uncertainty of group G3	**200**
G4 (Use of the detector under different experimental conditions):	
Spatial non-uniformity	40
Linearity correction	20
Temperature correction	10
Beam polarisation orientation	10
Temporal stability	20
Total uncertainty of group G4	**51**
Total	**211**

4.1.2 Amplification of a small photocurrent

Photocurrent amplifiers (current-to-voltage converters) are used both with the reference trap detector and with the filter radiometer. The filter radiometers are typically calibrated at a single power level but are used at several power levels with possibly quite large differences in the generated photocurrents. In this case, the gain-to-gain linearity of the preamplifier must be known with stated uncertainties. These separate current calibrations can be performed only if the detector and the preamplifier can be separated from each other.

The gain accuracy in the operational amplifier circuits is primarily determined by the accuracy and the temporal stability of the feedback resistors. Custom preamplifiers can be constructed with precision feedback resistors exhibiting low temperature and voltage coefficients of resistance. The shunt resistances of the detectors should be either measured or known so that the feedback resistances can be kept below the shunt resistances under operational conditions.

The preamplifiers can be calibrated using a precision current source whose output has been calibrated. These current sources can be calibrated using shunt resistors or by using a charging capacitor technique. The current source is operated to output a known current, and the voltage output of the preamplifier is measured using a calibrated voltmeter. This procedure can be repeated over the output range of the preamplifier at interval steps. A linear function can be fitted to the voltage output with changing input current to determine a single gain value and to determine the differences from linearity.

The uncertainties of the measurements include the uncertainties in the determination of the output current value from the current source. The input current should be stable between the time of the calibrations and the time of use. An additional source of uncertainty can arise from differences in the output resistance of the current source and the feedback resistance of the preamplifier. An example of such an uncertainty budget is shown in Table 2.

Table 2. Example uncertainty budget for the amplifier gain.

Uncertainty components 1×10^{10} V/A	Type	Relative uncertainty (ppm)
Current measurement	B	20
Short-term instability of input current	A	6
Voltage measurement (HP DVM, 3458A)	B	2
Output noise and drift (4 days)	A	16
Loop gain	A	2
Combined standard uncertainty of signal-gain, G_{amp}		26

4.1.3 Geometric propagation through a double aperture system

The geometric factor is defined by two apertures of known area, a known distance apart (Section 2.2).

4.1.3.1 Quality of the apertures and their area determination

To minimise the uncertainty associated with the two apertures, two things should be considered: the quality of the apertures and how the aperture areas are determined. Optically, a knife-edge aperture is ideal since it reduces scattering, but an aperture with a land (physical edge size) of 0.1 mm can be measured using a contact method. Diamond-turned aluminium, copper, or aluminium-bronze apertures have been found to have ideal properties for highly-accurate filter radiometry [10]. High-quality apertures can also be made from nickel over brass bi-metal substrate using electrochemical etching [11].

The aperture area can be determined using contact or non-contact methods. Typical stated uncertainties for contact methods (in the determination of diameter) are ~0.1 μm. However, there are two reasons not to 'believe' these uncertainties for operational use. The first is the results of the CCPR-S2 aperture comparison. As shown in Figure 6, the results did not agree within the uncertainties. This comparison compared optical and contact methods for measuring aperture area, and

there is a noticeable discrepancy. This suggests that uncertainties should be increased by at least a factor of 3.
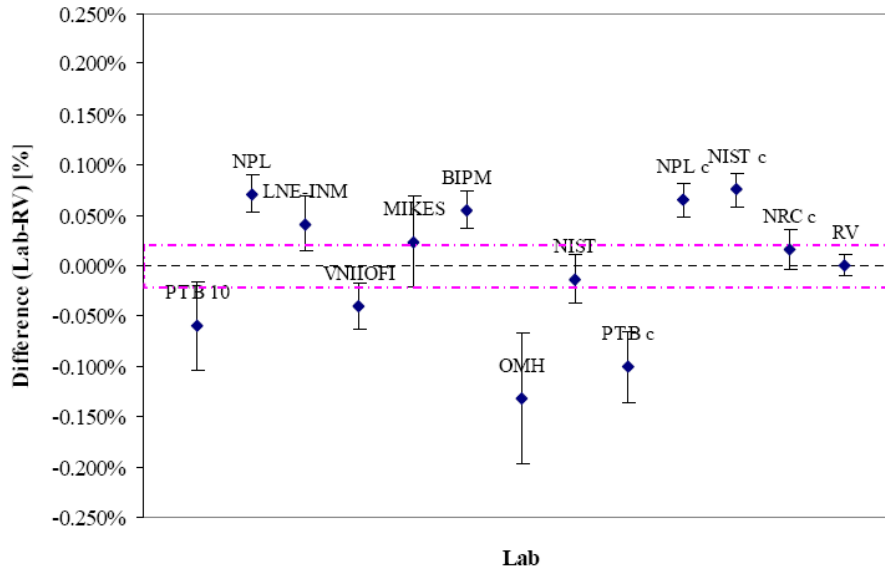
Figure 6. Comparison result for aperture area (from CCPR-S2 report).

The second reason that these uncertainties are likely to be under-estimated is that the measured values are based on calibrations of brand new apertures in the clean and very accurately temperature-controlled environment of a length metrology laboratory. Apertures in operational use in an optical or thermal laboratory (often with high-temperature graphite furnaces producing graphite dust) can often have minor damage. It is important to ensure that apertures near a high-temperature furnace are also temperature-controlled, for example by using a temperature-controlled aperture holder.

The geometric factor as used here is based on the radii of the two apertures. This makes an underlying assumption that the apertures are perfectly round. In practice, aperture roundness can vary and so needs to be determined during the measurements of diameter.

4.1.3.2 Alignment of the apertures

The calculation of the geometric factor assumes that the apertures are co-aligned. It is not unreasonable to assume that they may be slightly misaligned relative to each other, say by ~2 mm at 300 mm separation. Consider Figure 7. The distance between the two apertures is the hypotenuse $d/\cos\theta$. As irradiance drops according to the inverse square law, this means the irradiance of the second aperture is reduced compared to the on-axis irradiance by $\cos^2\theta$. The second aperture has an effective area in this direction of $A_2\cos\theta$ and the first aperture has an effective area of $A_1\cos\theta$. Combining all of this, the effective irradiance drops as $\cos^4\theta$. For $d = 300$ mm and $x = 2$ mm, $\cos^4\theta = 0.999911$. Therefore, the uncertainty associated with the measured radiance due to possible misalignment is < 0.009 %.

The apertures are aligned to be parallel with each other and perpendicular to the optical axis either by back-reflecting a laser beam or by aligning the apertures to the faces of a gauge bar. If the laser method is used, the angular uncertainty is approximately 0.0005 radians, which has a negligible effect

on the effective area. If a gauge bar is used, an angular uncertainty of 0.01 radians is reasonable, which leads to an uncertainty in the effective area of approximately 0.01 %.
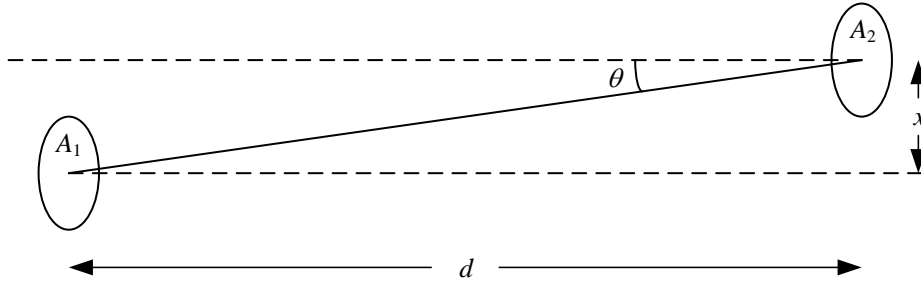
Figure 7. Geometry for misaligned apertures.

4.1.3.3 Distance between the apertures

To determine the distance between the apertures, a gauge bar of known length can be placed in between the two apertures and the apertures moved towards the bar, or a tubular vernier inside micrometer with adjustable extension rods can be used so that the gauge just touch the faces. Care must be taken not to damage the apertures when they are brought to touch the ends of the gauge bar. For higher accuracy, interferometry can be used. Since the geometric factor varies with the square of the distance between the apertures, lower uncertainties are achieved (for a given accuracy in the distance measurement) when the distance between the apertures is increased [12, 13].

4.1.3.4 Uncertainty associated with the geometric factor

The geometric factor is given by Eq. (5). If we define the variables

$$\beta = \sqrt{\left(r_1^2 + r_2^2 + d^2 \right)^2 - 4r_1^2 r_2^2} \tag{18}$$

and

$$\alpha = r_1^2 + r_2^2 + d^2 + \beta , \tag{19}$$

then

$$g = \frac{2\pi r_1^2 r_2^2}{\alpha} . \tag{20}$$

The sensitivity coefficients are given by:

$$\frac{\partial g}{\partial r_1} = \frac{4\pi r_1 r_2^2}{\alpha} \left[1 - \frac{r_1^2}{\alpha} \left(\frac{\alpha - 2r_2^2}{\beta} \right) \right], \tag{21}$$

$$\frac{\partial g}{\partial r_2} = \frac{4\pi r_1^2 r_2}{\alpha} \left[1 - \frac{r_2^2}{\alpha} \left(\frac{\alpha - 2r_1^2}{\beta} \right) \right], \tag{22}$$

and

$$\frac{\partial g}{\partial d} = \frac{-4\pi r_1^2 r_2^2 d}{\alpha\beta} . \tag{23}$$

Thus, the uncertainty in g (in m^2 sr), given the uncertainties in the radii and distances (in m), is:

$$u(g) = \left[\left(\frac{\partial g}{\partial r_1} u(r_1) \right)^2 + \left(\frac{\partial g}{\partial r_2} u(r_2) \right)^2 + \left(\frac{\partial g}{\partial d} u(d) \right)^2 \right]^{1/2}. \tag{24}$$

Note that the uncertainty in each radius is likely to be half that in the corresponding diameter measurement. For further calculation, it is useful to turn Eq. (24) into a relative uncertainty. This is done by dividing it by the value of g:

$$u_{\text{rel}}(g) = \frac{u(g)}{g}. \tag{25}$$

It should be noted that the area of an aperture and the diffraction from the aperture edge can change with time. Damage to the edge of an aperture will affect both the area and the amount of light diffracted from the edge.

Note that for both the irradiance method and the hybrid method of calibrating the filter radiometer, the area of the filter radiometer's aperture is taken into account in the irradiance responsivity determination.

4.1.3.5 Variation for irradiance and hybrid approach calibrations

For the hybrid and irradiance calibration approaches, the significant apertures are those on the trap detector and the additional aperture introduced (the lens aperture for the hybrid method or the source aperture for the irradiance method). The aperture on the filter radiometer is also important, but its absolute area does not need to be known with the same accuracy – although it is essential that it is stable.

The irradiance of the monochromatic irradiance field is measured with the trap detector (with its aperture). The irradiance responsivity of the filter radiometer, $s_{E,\text{FR}}$, is then determined by comparison with that of the trap detector using:

$$s_{E,\text{FR}}(\lambda) = \frac{S_{\text{cal,FR}}(\lambda)}{S_{\text{cal,trap}}(\lambda)} s_{\Phi,\text{trap}}(\lambda) A_{\text{trap}}, \tag{26}$$

where $S_{\text{cal,FR}}(\lambda)$ is the signal on the filter radiometer during calibration, $S_{\text{cal,trap}}(\lambda)$ is the signal on the trap detector, and $s_{\Phi,\text{trap}}(\lambda) A_{\text{trap}} = s_{E,\text{trap}}(\lambda)$ is the irradiance responsivity of the trap detector, determined from the flux responsivity $s_{\Phi,\text{trap}}(\lambda)$ and the trap aperture area A_{trap}.

When the filter radiometer is used, then the radiance responsivity is required, as in Eq. (9) or Eq. (10). The overall geometric term in combining Eq. (26) and Eq. (10) is

$$g_E = \frac{gA_{\text{trap}}}{A_{\text{FR}}} . \tag{27}$$

With the terms α and β as defined in Eqs (18) and (19), the equivalent of Eq. (24) is:

$$u(g_E) = \left\{ \left[\frac{4r_{\text{FR}} r_{\text{lens}}^2}{\alpha^2} \left(\frac{\alpha - 2r_{\text{lens}}^2}{\beta} \right) A_{\text{trap}} u(r_{\text{FR}}) \right]^2 \right.$$
$$+ \left[\frac{4r_{\text{lens}}}{\alpha^2} \left(1 - \frac{r_{\text{lens}}^2}{\alpha} \left(\frac{\alpha - 2r_{\text{lens}}^2}{\beta} \right) \right) A_{\text{trap}} u(r_{\text{lens}}) \right]^2 \tag{28}$$
$$\left. + \left[\frac{4r_{\text{lens}}^2 dA_{\text{trap}}}{\alpha\beta} u(d) \right]^2 + \left[\frac{4\pi g r_{\text{trap}}}{A_{\text{FR}}} u(r_{\text{trap}}) \right]^2 \right\}^{1/2} .$$

4.1.3.6 Uncertainties

Table 3 gives the normal and best uncertainties associated with the calculation of the geometric factor.

Table 3. Uncertainties associated with the calculation of the geometric factor.

Quantity	Standard uncertainty (relative, % or absolute)		Sensitivity coefficient for relative radiance	Relative standard uncertainty in radiance		Comments
	Normal	Best		Normal	Best	
Aperture radius	1 μm (radius)	0.5 μm (radius)	Eqs. (20) and (21)	0.02 %	0.01 %	Relative uncertainty in radiance based here on 3 mm and 5 mm apertures, 500 mm apart.
Distance	0.25 mm	10 μm	Eq. (22)	0.1 %	0.004 %	Relative uncertainty depends on absolute distance and aperture areas.
Aperture co-alignment	0.01 %	0.0001 %	1	0.01 %	0.0001 %	
Aperture angular alignment	0.01 %	Negligible	1	0.01 %	0	
Aperture non-roundness	0.06 μm (radius)	0.02 μm (radius)	Eqs. (20) and (21)	0.004 %	0.001 %	Relative uncertainty in radiance based here on 3 mm and 5 mm apertures, 500 mm apart.
Aperture changes since calibration	0.02 % (area)	Negligible	1	0.02 %	0	From potential damage and thermal expansion.

4.1.4 Wavelength scale

The filters in a filter radiometer are used to select a specific spectral region for the measurements of the blackbody radiances. Tuneable lasers or broadband sources with monochromators are used to determine either the relative or the absolute spectral responsivities of filter radiometers, and the wavelength uncertainties of these sources must be determined. If the wavelengths of the spectral responsivity determinations are in error, then, due to the spectral dependence of the Planck function, the calculated temperatures will also be in error.

Laser-based methods rely upon wavemeters to determine the wavelengths of the laser radiation. These wavemeters use interferometers with an internal laser that acts as a reference to determine the wavelength of the radiation. Wavemeters have the lowest uncertainties in the wavelength assignments but can only be used with coherent radiation, such as that from a laser.

Monochromators, which use gratings or prisms, are calibrated for their wavelength scales using a set of low-pressure atomic emission lamps. Atomic emission sources, such as Hg, Ne, Ar, Kr, and others, are used to generate a sufficient number of known spectral peaks. The wavelengths at which these atomic emission transitions occur are well known and published in atomic-transition databases. The uncertainty of these transition assignments is about 0.01 pm [7]. For the calibration of monochromators, these emission lamps should be placed in integrating spheres so that an angularly- and spatially-uniform radiation can be input into the monochromator. The radiation from the integrating sphere must fill both the fore optics and the internal optics of the monochromator. Care should also be taken to place the exit of the integrating sphere source at the position of the lamp or the broadband source that is typically used to illuminate the monochromator. If the emission source is shifted from the position of the broadband source, the wavelength calibration will be shifted due to the different angular position of the atomic emission source as compared to that of the broadband source.

The angular positions of the grating or prism disperser can be measured using an optical rotary encoder attached to the shaft of the threaded rod or, preferably, an angular encoder. The spectral peak position is determined using the centroid calculated from the measured spectral signal. The centroid can shift depending on the wavelength extent over which the summation is performed. A symmetric wavelength interval should be chosen for the summation range for the centroid calculations.

The wavelength accuracy of monochromators can be improved by using a piece-wise polynomial fit, which minimises the residuals of the fit. The order of the polynomial can be increased until the residuals from the fit do not decrease in substantive ways.

The uncertainties of the wavelength calibrations are determined from the standard deviation of the residuals of the polynomial fitting function from the actual atomic emission line wavelength assignments. The wavelength accuracies can be further checked using a spectrograph that has also been calibrated for wavelength measurements.

The laser-based method, where the laser wavelengths are determined using a wavemeter, will not require any corrections. Table 4 gives the normal and best uncertainties for monochromator and laser-based measurement systems.

Table 4. Uncertainties in wavelengths measured using both laser-based and monochromator-based systems.

Quantity	Standard uncertainty	
	Normal	Best
Laser wavelengths	3.0 pm	0.1 pm
Monochromator wavelengths	100 pm	20 pm

4.1.5 Out-of-band radiation

Out-of-band (OOB) suppression of radiation is more critical for thermodynamic temperature measurements than for measurements under ITS-90. This is because under ITS-90 the ratio of the radiances of two blackbodies is measured and the OOB error for each measurement partially cancels. However, for thermodynamic measurement, the filter radiometer is calibrated using an integrating sphere that is illuminated using a monochromatic source. In this case, the radiance of the integrating sphere is compared to the radiance of a blackbody. OOB radiation will cause the response of the filter radiometer in front of the blackbody to be higher than expected, because the radiance of a blackbody is integrated over the full bandwidth of the detector, which is not the case during calibration with the monochromatic source. The transmittance in the far wings of the spectral responsivity should, therefore, be evaluated to estimate the OOB correction.

Unaccounted-for OOB transmittance causes the measured signal to be higher than expected by the factor K_{OOB} (see Eq. (12)), given by

$$
\begin{aligned}
K_{\mathrm{OOB}} &= 1 + \frac{\int_0^{\lambda_1} s(\lambda) L_{\mathrm{b}}(\lambda,T) d\lambda + \int_{\lambda_2}^{\infty} s(\lambda) L_{\mathrm{b}}(\lambda,T) d\lambda}{\int_{\lambda_1}^{\lambda_2} s(\lambda) L_{\mathrm{b}}(\lambda,T) d\lambda} \\
&= \frac{\int_0^{\infty} s(\lambda) L_{\mathrm{b}}(\lambda,T) d\lambda}{\int_{\lambda_1}^{\lambda_2} s(\lambda) L_{\mathrm{b}}(\lambda,T) d\lambda},
\end{aligned}
\tag{29}
$$

where λ_1 and λ_2 are the practical wavelength limits over which the integral in Eq. (13) is evaluated.

To avoid OOB corrections, the requirements for OOB suppression depend on the centre wavelength of the spectral responsivity function and the spectral bandpass. The OOB analysis given here is for a filter radiometer with a spectral filter centred at 650 nm and a spectral bandwidth of 10 nm used with a Si detector, which is a common configuration used in national metrology institutes (NMIs). Note that the OOB analysis can be carried out using relative spectral responsivities.

A spectral filter should be measured separately prior to its incorporation into a radiometer, to determine whether its OOB suppression is sufficient. Depending on the filter radiometer design, possible radiation leakage around the filter could be perceived as OOB radiation even though the light path does not go directly through the filter. A comparison of the expected component-wise responsivity and the actual spectral responsivity of the filter radiometer as a whole is helpful in assessing any possible light leakage in the filter radiometer.

Measurements of the OOB response of spectral responsivities to high optical densities are difficult to perform using traditional monochromator and lamp sources because of their low power outputs, and measurements of filter response to optical densities higher than 5 (OD5) using commercial spectrophotometers are challenging. Some filter manufacturers have recently started offering better than OD6 OOB suppression [14]. Custom-designed transmittance setups using high-power supercontinuum lasers and monochromators have led to OOB measurements down to OD8 [15] and even OD11 [16].

The temperature error, ΔT, resulting from uncorrected OOB radiation can be calculated as

$$\Delta T \approx \left(K_{\text{OOB}} - 1\right) \frac{n\lambda_0 T^2}{c_2}, \tag{30}$$

where λ_0 is the mean wavelength of the filter radiometer's spectral responsivity, and the monochromatic and Wien's approximations have been used. Assuming a filter radiometer consisting of a 10 nm bandwidth rectangular spectral filter centred at 650 nm, with a Si photodiode that is sensitive to radiation within its entire spectral range from 200 nm to 1100 nm, Eq. (29) can be used to calculate the value of K_{OOB}. The worst case is when the OOB radiation is flat across the entire spectral range, in which case the value of $K_{\text{OOB}} - 1$ at 1300 K is given by $1136 \times 10^{-\text{OD}}$ and at 3000 K is given by $76.51 \times 10^{-\text{OD}}$, where OD is the optical density value of the filter. This gives rise to temperature errors, given by Eq. (30), of $86700 \times 10^{-\text{OD}}$ K at 1300 K and $31106 \times 10^{-\text{OD}}$ at 3000 K (e.g., temperature errors of 0.87 K and 0.31 K, respectively, for a filter with OOB suppression of OD5). Thus, OOB suppression beyond OD7 will result in errors less than about 9 mK at 1300 K and about 3 mK at 3000 K.

An alternative method to determine the OOB correction is to use a notch filter to cut out the in-band signal of the filter radiometer. The value of K_{OOB} can then be determined by measuring the filter radiometer signal, S, with and without the notch filter in place:

$$K_{\text{OOB}} \approx 1 + \frac{S_{\text{with notch filter}}}{S_{\text{without notch filter}}}. \tag{31}$$

This method relies on high transmittance of the notch filter outside the notch region and low transmittance inside. Corrections to Eq. (31) can be made if these transmittances are known.

4.1.6 Stray light

Stray light is defined as detected photons that do not propagate along a straight line from the source to the radiometer. Optical diffusion by the molecules of the atmosphere is neglected here, and stray light is considered to originate only from optical diffusion of the source used to illuminate the radiometer. Stray light causes the detected flux, $\Phi(d)$, to differ from that given by Eq. (6); note the explicit dependence here of Φ on the distance, d, between the source and detector apertures. The stray detected flux, $\Phi_{\text{stray}}(d)$, may be defined as:

$$\Phi_{\text{stray}}(d) = \Phi(d) - \Phi_0(d), \tag{32}$$

where $\Phi_0(d)$ is the stray-light-free flux given by Eq. (6):

$$\Phi_0(d) = g\pi L_0, \tag{33}$$

where L_0 is the radiance of the source.

In the absence of stray light, the detected flux is given by $\Phi(d) = \Phi_0(d)$. At the other extreme, the stray light would be maximised if the optical beam were enclosed within a perfect light pipe. In this case, the detected flux would be constant and independent of d. The real situation will be somewhere between these two extremes, and we can propose that the stray light is approximately inversely proportional to d:

$$\Phi_{\text{stray}}(d) \approx kdg\pi L_0, \tag{34}$$

where k is a constant (note that the geometric factor, g, given by Eq. (5), is approximately inversely proportional to d^2 when the aperture separation is much greater than the radii of the two apertures).

Equation (32) can be converted to the filter radiometer signal (as in Eq. (13)):

$$S(d) = S_0(d) + S_{\text{stray}}(d), \tag{35}$$

where $S(d)$ is the total measured signal as a function of distance, $S_0(d)$ is the stray-light-free component of the signal, and $S_{\text{stray}}(d)$ is the component of the signal corresponding to the stray light. Using Eqs (33) and (34), Eq. (35), after dividing both sides by g, can be written

$$\frac{S(d)}{g} = \frac{S_0(d)}{g}(1 + kd). \tag{36}$$

Note that the quantity $S_0(d)/g$ is independent of d, so fitting a straight line to the measured signal divided by g as a function of distance allows S_0 and k to be evaluated from the intercept and slope, respectively. The correction factor for stray light, K_{stray} (see Eq. (12)), is given by:

$$K_{\text{stray}} = 1 + kd, \tag{37}$$

where d is the distance used for the blackbody temperature measurement.

The uncertainty in the value of k can be determined using the standard formulae for straight-line fitting, and depends on the sampling of the distance d:

$$u^2(k) \approx \left[\left(\frac{u(S(d))}{S(d)} \right)^2 + \left(\frac{u(g)}{g} \right)^2 \right] \frac{1}{\sum_{i=1}^{N} d_i^2 - \frac{1}{N} \left(\sum_{i=1}^{N} d_i \right)^2}, \tag{38}$$

where the distance has been sampled at N values, d_i, and it has been assumed that the uncertainty $u\left(S(d)/g\right)$ is the same for each measurement and the uncertainties in the distance measurements are negligible. Thus, the relative uncertainty in the stray-light correction factor, K_{stray}, is

$$\frac{u(K_{\text{stray}})}{K_{\text{stray}}} = \left[\left(\frac{d}{1+kd}u(k)\right)^2 + \left(\frac{k}{1+kd}u(d)\right)^2\right]^{1/2}. \tag{39}$$

4.1.7 Diffraction and aperture scatter

Diffraction effects at the apertures lead to a deviation δ between the measured radiation flux, Φ_{rad}, and the flux calculated by means of geometrical optics, Φ_{geom}:

$$\Phi_{\text{rad}} = \left(1+\delta\right)\Phi_{\text{geom}}. \tag{40}$$

Generally, the deviation δ is small for a large ratio of aperture diameter to wavelength [17], but can have a positive or negative sign. For typical experimental setups in radiometry, where the radiation overfills the aperture, δ becomes positive and is generally $\ll 1$.

For the different calibration approaches, diffraction will be considered in different places:
- For the power method, diffraction is significant for the apertures used during the blackbody measurement.
- For the irradiance method, diffraction is significant for the apertures used during the blackbody measurement.
- For the hybrid method, diffraction effects are part of the absolute SSE and are not considered separately.
- For the radiance method, diffraction is significant for the apertures used with the trap detector for calibration. Diffraction in the filter radiometer is part of the relative SSE and is not considered separately.

Diffraction occurs for both of the two apertures that define the optical geometry. As both effects are small, they can be treated independently, and the two corrections add to give:

$$\delta_{\text{aperture},1+2} = \delta_{\text{aperture},1} + \delta_{\text{aperture},2}. \tag{41}$$

Hence, the following two cases can be treated separately:
1. Diffraction at the filter radiometer's aperture: the furnace aperture acts as a source and the photodiode as an under-filled detector.
2. Diffraction at the furnace aperture: the opening of the blackbody radiator acts as a source and the filter radiometer aperture as an over-filled detector.

Invoking the reciprocity theorem of Kirchhoff, the deviation due to diffraction does not change if the source and detector are exchanged. Therefore, the two cases can be treated as equivalent. References [18, 19] give both exact solutions and approximations for this diffraction problem.

For a blackbody source, the diffraction correction must be calculated for all wavelengths measured. The radiometers typically used only have a small bandpass of 10 nm to 20 nm. The diffraction correction δ is inversely proportional to the wavelength and varies little across the bandpass. For simplification, often only the centre wavelength of the interference filter is used in the calculation of the correction. While a furnace aperture diameter of 20 mm is typically used for the standard measurement of a high-temperature blackbody's temperature using a filter radiometer, a large eutectic fixed-point cell with 8 mm cavity diameter requires a furnace aperture of 3 mm in diameter, which results in a considerably larger diffraction effect because of the smaller furnace aperture.

By changing the distance between the two apertures, the chosen approximation for the diffraction correction can be experimentally tested and an uncertainty of the correction can be deduced. This has been found to be of the order of 2×10^{-4}.

4.2 Sources of Uncertainty Specific to the Calibration Scheme

4.2.1 Power approach

In order to measure temperature using a filter radiometer (FR) calibrated via the power method, two steps are required. First, the power responsivity of the FR needs to be determined. Then, the measurement geometry is defined using two apertures of known areas and known separation (see Figure 1).

To calibrate the absolute spectral responsivity of a filter radiometer using the power method, a beam of quasi-monochromatic radiation under-fills the FR aperture and a transfer detector (trap or single element) is used as a reference. The transfer detector will have had its spectral responsivity calibrated with respect to an absolute standard (cryogenic radiometer or other absolutely-calibrated detector). Typically, a monochromator is used to provide the quasi-monochromatic beam and mirrors are used to image the monochromator's output slits onto the FR and the transfer detector. The transfer detector is used to measure the power in the beam and then the FR is moved into place in front of the beam and its output is measured. The monochromator wavelength is changed, and the measurements are repeated until the wavelength range of the FR has been measured (see Figure 8).
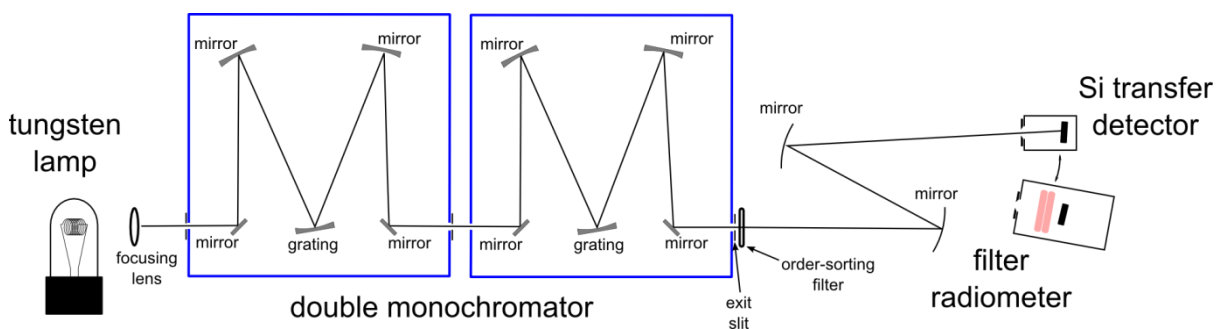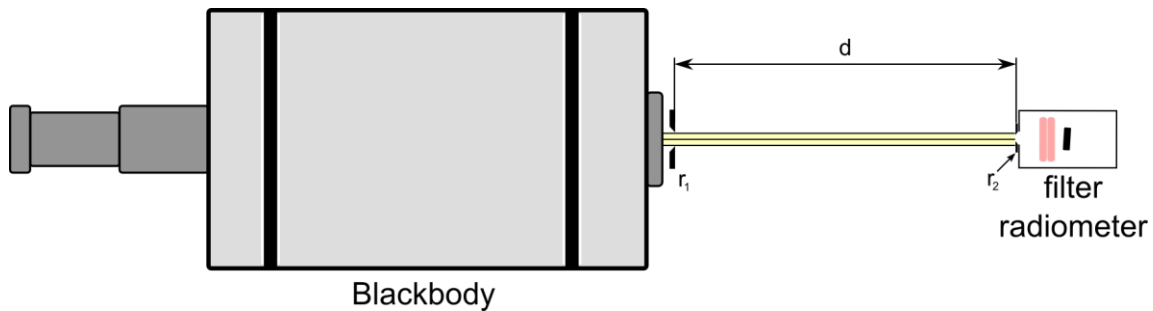
Figure 8. Calibration and use setups for the power method.

With the power responsivity known, apertures can be added to the system to enable the radiance measurement to be made, which can then be converted to temperature. Equation (13) can be solved iteratively to obtain the temperature, with the radiance responsivity defined by Eq. (8).

Additionally, it is necessary to know or verify the uniformity of the FR and transfer detector since the calibration geometry is different from the in-use measurement geometry. This can be done by rastering a focused beam across the entrance aperture of the FR. Boivin [20] has described this method for trap- and single-element Si detectors and found a uniformity of 0.05 %. For a filter radiometer it is also important that the filter is uniform.

4.2.1.1 Sources of uncertainty for the power method

The common sources of uncertainty, described in Section 4.1, apply to the power method as follows:
- The uncertainty in the power responsivity of the trap detector impacts directly on the uncertainty in the power responsivity of the filter radiometer.
- The uncertainty in the gain of the transimpedance amplifiers must be considered for the trap amplifier during calibration and, if a different gain is used for calibration and use of the filter radiometer because of different signal levels, for the filter radiometer as well.
- The geometric factor is derived from the two apertures added to the system for measuring a blackbody. The uncertainty analysis follows that described in Section 4.1.3.4, and the uncertainty in the geometric factor is given by Eq. (24).
- The wavelength scale is based on the monochromator used to provide the quasi-monochromatic beam.
- Out-of-band transmittance must be considered, as described in Section 4.1.5.
- Stray light is relatively straightforward to control during calibration because the monochromator provides a beam of radiation.

In addition, it is necessary to consider:
- The uncertainty associated with the uniformity of the filter radiometer and the average response over the area illuminated by the calibration beam and the area of the aperture used.
- Diffraction at the apertures during the blackbody measurement.

4.2.2 Irradiance approach

The spectral irradiance responsivity of the filter radiometer with mounted aperture is determined with a calibrated trap detector together with a calibrated entrance aperture defining the effective area of the trap detector. The spectral irradiance responsivity can be determined with a monochromator-based [5, 6] or a laser-based [3, 21] system. During use, an additional aperture is added in front of the

blackbody to define the solid angle necessary to convert from irradiance to radiance (see Figure 2). Absolute primary thermometry from the Zn point upwards has been performed by this method [22–26]. However, diffraction losses increase drastically for a decreasing diameter of the furnace aperture, so the method has been adapted, as in the hybrid method below, for determining the temperature of small sources (e.g., high-temperature fixed points (HTFPs)) [27–29].

4.2.2.1 Sources of uncertainty for the irradiance method

The common sources of uncertainty, described in Section 4.1, apply to the irradiance method as follows:

- The uncertainty in the power responsivity of the trap detector impacts directly on the uncertainty in the irradiance responsivity of the filter radiometer.
- The uncertainty in the gain of the transimpedance amplifiers must be considered for the trap amplifier during calibration and, if a different gain is used for calibration and use of the filter radiometer because of different signal levels, for the filter radiometer as well.
- The geometric factor is derived from the filter radiometer and the aperture added to the system for measuring a blackbody. However, because the radiometer is calibrated for irradiance responsivity, the aperture on the trap detector is more significant than that on the filter radiometer. The uncertainty analysis follows that described in Section 4.1.3.5, and the uncertainty in the geometric factor is given by Eq. (28).
- The wavelength scale is based on the monochromator or laser used to provide the irradiance field used in the calibration.
- Out-of-band transmittance must be considered, as described in Section 4.1.5.
- The significance of stray light in the calibration depends on the method used to generate the irradiance field.

In addition, it is necessary to consider:

- The uncertainty associated with the uniformity of the irradiance field used and the relative sizes of the filter radiometer and trap apertures (and how much they are aligned in the same position within that irradiance field).
- Diffraction at the apertures during the blackbody measurement.

4.2.3 Hybrid approach

The irradiance approach can be applied to smaller blackbody cavities by introducing a single lens to create the hybrid method [30]. The calibration is usually performed "in parts", with the irradiance responsivity of the filter radiometer determined as above, and the transmittance of the lens determined separately [3, 31]. Again, an additional aperture is added to the lens to form the geometric system for radiance (see Figure 3). Formally, the method can be considered equivalent to the irradiance method above, but is capable of measuring sources with small apertures. Note that here it is important that the irradiance field is formed by a light source converging with the same geometry as the lens provides – this ensures that the filter is illuminated with the same range of angles in calibration and use. Usually this is achieved by imaging a source, e.g., a laser-illuminated integrating sphere, using the same lens system.

The calibration process assumes that the same irradiance is measured by the trap detector and filter radiometer. This relies on the spatial uniformity of the source and any differences, or potential differences, in the sizes of the two apertures and their position within the uniform irradiance field. The source also needs to be stable between the trap measurement and the filter radiometer measurement. Angular uniformity is less critical, although it is important that the irradiance field matches the geometry that will be used for measurements with the lens so that the filter is illuminated with the same range of angles.

Generally, the irradiance field is created by imaging a small aperture on an integrating sphere. There is usually a compromise to be made, where a larger integrating sphere will create a more spatially uniform image but will have a lower irradiance level for the same input laser power, and this will make the signal more noisy and limit how far into the wings of the filter radiometer spectral responsivity measurements can be made.

With a hybrid-mode calibration, with the irradiance field created by imaging a sphere exit port, stray light can generally be very well limited by placing the imaging lens in a large baffle screen. After the lens, the main light is well controlled and unlikely to scatter. Dark readings can be taken by closing the lens. The hybrid-mode calibration, therefore, has very low sensitivity to stray light.

The lens transmittance of a simple uncoated lens can be reasonably predicted from the Fresnel equations. More accurate results can be obtained [31] by treating the Fresnel prediction as a relative spectral transmittance and making measurements at a single wavelength to provide an absolute scaling.

In most applications, the size-of-source effect (see Section 6.1.2) is a relative effect: the instrument is sensitive to the *difference* in the size (and lateral uniformity) of the test and reference sources. For the hybrid method it is an absolute effect. Because the filter radiometer is calibrated without a lens, there is no reference source size[2], and what matters is the absolute size-of-source effect, i.e., the difference when viewing the test source compared to an infinite uniform source. This is difficult to estimate, and it is even more difficult to estimate an uncertainty for it, although for a hybrid-mode calibration this is often the dominant uncertainty. It is necessary to make SSE characteristic measurements out to sufficiently large sources that the SSE characteristic of the instrument flattens off.

One solution [32], which avoids the use of an absolute SSE, is to calibrate the lens transmittance and SSE simultaneously by making measurements of a large-aperture radiance source both with and without the lens. If the SSE and lens transmittance are determined separately, they have typical normal standard uncertainties of 0.06 % and 0.04 %, respectively [30]. If they are measured together then smaller standard uncertainties are achievable [32].

4.2.3.1 Sources of uncertainty for the hybrid method
The common sources of uncertainty, described in Section 4.1, apply to the hybrid method as follows:
- The uncertainty in the power responsivity of the trap detector impacts directly on the uncertainty in the irradiance responsivity of the filter radiometer.

---

[2] Note, that a lens may be used in creating the irradiance source for the calibration. But since both the trap detector and filter radiometer are on the same side of that lens, any SSE is cancelled in calibration.

- The uncertainty in the gain of the transimpedance amplifiers must be considered for the trap amplifier during calibration and, if a different gain is used for calibration and use of the filter radiometer because of different signal levels, for the filter radiometer as well.
- The geometric factor is derived from the filter radiometer and the lens apertures. However, because the radiometer is calibrated for irradiance responsivity, the aperture on the trap detector is more significant than that on the filter radiometer. The uncertainty analysis follows that described in Section 4.1.3.5, and the uncertainty in the geometric factor is given by Eq. (28).
- The wavelength scale is based on the laser used to provide the irradiance field.
- Out-of-band transmittance must be considered, as described in Section 4.1.5.
- Stray light is relatively straightforward to control during calibration because the lens used to obtain the same geometry for calibration and filter radiometer use controls the direction of radiation.

In addition, it is necessary to consider:
- The uncertainty associated with the uniformity of the irradiance field and the relative sizes of the filter radiometer and trap apertures (and how much they are aligned in the same position within that irradiance field).
- The calibration of the transmittance of the lens.
- The absolute SSE.

4.2.4 Radiance approach

An appropriately designed imaging radiometer can be calibrated in absolute mode as a radiance-mode filter radiometer. The more complex optical system of the thermometer (e.g., several lenses and appropriate baffling) can lead to an extremely low size-of-source effect [33–35].

The calibration of such a system is by comparison with a source of known radiance, as shown in Figure 4. The instrument can then be used to determine the blackbody radiance directly. Examples of the method can be found in [34–36]. Briefly, the radiation thermometer is calibrated against a cryogenic radiometer by the use of silicon trap detectors that are calibrated for power responsivity at selected wavelengths. The full responsivity is then determined by interpolation. The spatial uniformity of the trap detector is utilised to obtain the irradiance responsivity from the power responsivity in conjunction with a precision aperture. If the geometric parameters, such as the aperture area and the distance between the integrating sphere and the trap detector, are known, then the spectral irradiance of the sphere source can be assigned. If the area of the precision aperture on the integrating sphere is known, then the spectral radiance of the sphere can be determined. Radiation thermometers are calibrated as a system without separately measuring the transmittance of the lenses and characteristics of the components. The calibrations are performed at many different wavelengths with stabilised lasers.

The common sources of uncertainty, described in Section 4.1, apply to the radiance method as follows:
- The uncertainty in the power responsivity of the trap detector impacts directly on the uncertainty in the radiance responsivity of the filter radiometer.
- The uncertainty in the gain of the transimpedance amplifiers must be considered for the trap amplifier during calibration and, if a different gain is used for calibration and use of the filter radiometer because of different signal levels, for the filter radiometer as well.

- The geometric factor is derived from the two apertures added to the trap detector and the integrating sphere for measuring the monochromatic radiance source. The uncertainty analysis follows that described in Section 4.1.3.4, and the uncertainty in the geometric factor is given by Eq. (24).
- The wavelength scale is based on the laser used to illuminate the radiance source.
- Out-of-band transmittance must be considered, as described in Section 4.1.5.
- Stray light can be challenging to control, especially if the first aperture is mounted on the integrating sphere.

In addition, it is necessary to consider:
- The uncertainty associated with the uniformity of the integrating sphere – both spatial and angular uniformity.
- Diffraction at the apertures used to measure the integrating sphere. This is reduced when the first aperture is closer to the integrating sphere (but in turn this increases stray light).

5. Other Characteristics of the Filter Radiometer

5.1 Spectral Selection and Filtering

The spectral selection for the filter radiometer can be made with interference filters, with glass filters, or with a monochromator (prism or grating). There are uncertainties associated with both the calibration and use of the filter radiometer that depend on the chosen filtering approach.

5.1.1 Glass and interference filters

Interference filters applied as wavelength selecting elements in filter radiometers are susceptible to changes in their spectral transmittance properties (i.e., the centre wavelength and the integrated transmittance), mainly due to modifications of the optical pathlengths within the constituent dielectric material thin layers [37]. These modifications have their origin in filter temperature changes, angular incidence dependence, water vapour absorption, and irreversible changes due to ageing.

For the assessment of the uncertainty contributions due to these effects, Eq. (13) in Section 2.5 is used:

$$S = K \int_0^\infty s(\lambda) L_b(\lambda, T) d\lambda \,. \tag{42}$$

For filter radiometers with narrowband interference filters, S can be approximated as:

$$S \approx K L_b(\lambda_0, T) \int_0^\infty s(\lambda) d\lambda \approx K L_b(\lambda_0, T) I_s \,, \tag{43}$$

where I_s is the integrated spectral responsivity and λ_0 is the mean wavelength according to:

$$\lambda_0 = \frac{\int_0^\infty \lambda s(\lambda) d\lambda}{\int_0^\infty s(\lambda) d\lambda} \,. \tag{44}$$

When the spectral responsivity is symmetric, λ_0 is equal to the centre wavelength.

5.1.1.1 Sensitivity to temperature

Typically [1], with increasing temperature, the mean wavelength of an interference filter is shifted towards longer wavelengths whilst the integrated transmittance I_s decreases (see Table 5). When considered as a unit with a silicon photodiode detector (i.e., a filter radiometer) and operated close to the bandgap wavelength range of the detector, the temperature coefficient of the integrated spectral responsivity is dominated by the temperature coefficient of the detector (see Table 6).

Table 5. Change in integrated transmittance, I_s, and mean wavelength, λ_0, per temperature change for a range of interference filters.

Interference Filter	$\left(\Delta I_s/I_s\right)\big/\Delta T$ (K^{-1})	$\Delta\lambda_0/\Delta T$ (pm·K^{-1})
IF450	-3.4×10^{-4}	15
IF500	-3.1×10^{-4}	17
IF650	-4.3×10^{-4}	20
IF800	-7.9×10^{-5}	26
IF900	-9.0×10^{-5}	27

Table 6. As for Table 5, but including the temperature coefficient of a silicon photodiode (i.e., for a complete filter radiometer).

Filter Radiometer	$\left(\Delta I_s/I_s\right)\big/\Delta T$ (K^{-1})	$\Delta\lambda_0/\Delta T$ (pm·K^{-1})
FR800	-2.8×10^{-4}	33
FR900	0.2×10^{-4}	30
FR1000	13.5×10^{-4}	35

Under the assumption that Wien's approximation to Planck's law can be applied (VIS/NIR spectral range), when measuring a blackbody at the temperature T, the change, ΔT, in the measured temperature due to a filter/detector temperature-change-caused centre wavelength shift $\Delta\lambda_0$ is equal to:

$$\Delta T \approx \frac{T}{\lambda_0}\left(5\frac{n\lambda_0 T}{c_2}-1\right)\Delta\lambda_0.\tag{45}$$

The associated uncertainty can then be calculated by assuming that the interference filter/detector temperature can be controlled within ±200 mK (normal) or ±50 mK (best). Extensive details on how uncertainties in the properties of the filter radiometer's spectral responsivity propagate to the measured temperature are given in Appendices A and B.

5.1.1.2 Sensitivity to angle of incidence

As the transmittance and the centre wavelength of an interference filter change with the angle of incidence of the optical radiation, and, in general, the beam geometry during calibration (e.g., collimated) is different from that during the application (e.g., divergent/convergent), these changes must be taken into account in the uncertainty budget. For incident angles, θ, smaller than 20°, the centre wavelength change, $\Delta\lambda_0$, can be expressed as [38]:

$$\Delta\lambda_0 = -\lambda_0 \frac{\theta^2}{2\mu_{\text{eff}}^2} , \tag{46}$$

where μ_{eff} is the "effective refractive index" of the interference filter. Equation (45) can be used to convert this to a change in measured temperature.

5.1.1.3 Stability/Ageing

The stability of interference filters with respect to observed ageing effects, in terms of the shift of the centre wavelength and modifications of the spectral transmittance, has its origin in:
- modifications of the structure of the dielectric thin film layers [39];
- absorption of water (moisture) by the dielectric thin film layers [40];
- contamination of the interference filter's outer surfaces.

The first effect can be ascribed to crystal growth in the (initially amorphous) deposited thin film dielectric layers. This time-dependent *irreversible* process causes a change of the refractive index and, hence, a shift of the centre wavelength towards longer wavelengths. The magnitude of the wavelength shift, which can be up to 1 % of the centre wavelength, depends on the thermal history (i.e., the substrate temperature during the manufacturing process of the interference filter). By choosing an adequate substrate temperature ($> 130\,°C$) during the thin film deposition process, and/or if the interference filter undergoes a subsequent heat treatment ($\sim 90\,°C$), the wavelength shift can be minimised [39]. Considering that interference filter technology has evolved, especially in terms of process control, and that the timescale of the described effect is of the order of tens of hours, the wavelength shift due to a crystallization process within the dielectric thin film layers can be neglected when assessing the mid- and long-term stability.

Due to the "sponge-like" fractal structure of the deposited thin film dielectric layers, the layers have a 10 % to 20 % (depending on the layer material) void space porosity, which makes them susceptible to the absorption of water. By absorbing moisture, the refractive index increases and consequently the centre wavelength is shifted towards *longer* wavelengths. Under the assumption that this process is *reversible*, it has been shown [40] that if interference filters previously exposed to environmental humidity undergo a thermal treatment (heating up to $70\,°C$), the water can be removed from the pores of the layers. This leads to a decrease of the refractive index and, consequently, the centre wavelength will shift back towards *shorter* wavelengths. Depending on the layer materials, the magnitude of the observed wavelength shift varies from 0.1 % to 0.5 % of the centre wavelength. If the interference filter is sealed against environmental humidity, the observed wavelength shift is considerably lower (< 0.01 % of the centre wavelength).

A different way to assess the stability of interference filters was followed in [41], and comprised an analysis of the calibration history of four different filter radiometers (FR) equipped with sealed, narrowband interference filters (centre wavelengths at 677 nm, 802 nm, 903 nm, and 1003 nm, FWHM: 14 nm to 24 nm) in terms of the temporal change of the centre wavelength and the integrated spectral responsivity over a period of approximately 8 years. Over this period, the FRs were routinely used to measure the thermodynamic temperature of blackbodies in the temperature range from $1000\,°C$ to $3000\,°C$. When not being used, the FRs were kept under cleanroom conditions but *not* under humidity-controlled conditions; i.e., they were exposed to the seasonal humidity variation of the laboratory. For the period investigated, all the FRs displayed a linear shift of the centre wavelength towards longer wavelengths, ranging from 0.038 nm per year to 0.067 nm per year, corresponding to a

maximum relative wavelength change of 0.01 % per year. Except for one FR, the integrated spectral responsivity over the bandpass of all the FRs did not change significantly; the relative changes observed in the assessed time interval were within the uncertainty of the calibration. For the FR with the centre wavelength at 677 nm, a sudden relative drop of 2×10^{-3} in the integrated spectral responsivity was observed. After cleaning of the interference filter, the integrated responsivity returned to the previous value, revealing contamination as the origin of the observed effect.

5.1.1.4 Fluorescence

Depending on the type of filter glass selected as the substrate in the interference filter, and on the spectral distribution of the radiation source the interference filter is exposed to during its application, the interference filter can display a significant fluorescence effect originating from the glass substrate and/or the optical cement. Although glass manufacturers specify in their catalogues whether the filter glasses are (non-)fluorescent, except for custom-made interference filters, details on the internal glass/optical cement setup of interference filters are not always available from the filter manufacturer. If fluorescence is suspected, that is if an apparent increasing transmittance towards shorter wavelengths is observed during the filter characterisation, special experimental care must be taken when these interference filters are applied in conjunction with high-temperature blackbodies. Generally, there is no analytical correction possible, but several (experimental) solutions have been presented to minimise the problem [42]. The most accessible solution from the radiation thermometry point of view is the following: because the fluorescent radiation is emitted in all directions, independently of the (directional) incoming radiation from the source, a careful design of the detector optical layout (i.e., the position of the interference filter) can minimise the contribution of fluorescence to the detector signal.

5.1.2 Monochromator-based filtering

The spectral selection can be achieved by a monochromator. The advantages of a monochromator are that it offers the possibility of adapting to the spectral range in which a monochromatic source (laser) is available, and the ease of the wavelength calibration using spectral lamps if multiple laser wavelengths are not accessible. The disadvantages are mainly the poor stability, the out-of-band stray light, and the large dimensions and weight, which make it difficult to transport.

Radiance comparators based on monochromators can be absolutely calibrated against a reference trap detector (with the necessary apertures of known area and distance, forming an ensemble called a "radiance meter" or "spectroradiometer"), but this calibration may not be valid for long periods due to insufficient stability of the monochromator. The radiance measurement would, therefore, become part of the measurement scheme in all cases. This method was applied in the past to the measurement of the thermodynamic temperature of the fixed point of copper [3, 4]. It is a direct radiance measurement method using a tuneable laser associated with an integrating sphere as a monochromatic source with a Lambertian distribution of the radiation.

The determination of the spectral responsivity of the monochromator with the corresponding slits (in other words, the slit function) is a major part of the measurement process.

5.1.2.1 Slit scattering function

The spectral responsivity of the spectroradiometer depends on the orientation of its optical grating via its slit scattering function $R_{\text{slit}}(\lambda - \lambda_{\text{eff}})$, where the effective wavelength λ_{eff} is defined by averaging

the slit scattering function distribution, $R(\lambda)$, weighted by the wavelength (i.e., λ_{eff} is the mean wavelength of the slit function):

$$\lambda_{\text{eff}} = \frac{\int_0^\infty \lambda R(\lambda) d\lambda}{\int_0^\infty R(\lambda) d\lambda} . \tag{47}$$

Because the spectral width of the slit scattering function of the monochromator is typically narrow (a few nm), the optical responsivity, $R_{\text{opt}}(\lambda)$, of the monochromator should not vary significantly throughout the bandwidth. Within this approximation, one can write the spectral responsivity of the spectroradiometer as a product of the slit scattering function of the monochromator multiplied by a smooth optical responsivity:

$$R(\lambda, \lambda_{\text{eff}}) = R_{\text{slit}}(\lambda - \lambda_{\text{eff}}) R_{\text{opt}}(\lambda). \tag{48}$$

The slit scattering function of the spectroradiometer $R_{\text{slit}}(\lambda - \lambda_{\text{eff}})$ is recorded with a laser of radiance $L_{\text{laser}}(\lambda) = L_0(\lambda_{\text{laser}})\delta(\lambda - \lambda_{\text{laser}})$, where λ_{laser} is the laser wavelength (in air) and δ is the Dirac delta function, and can be defined as a function of the voltage delivered by the spectroradiometer:

$$R_{\text{slit}}(\lambda_{\text{laser}} - \lambda_{\text{eff}}) = \frac{U_{\text{laser}}(\lambda_{\text{laser}} - \lambda_{\text{eff}})}{I_0(\lambda_{\text{laser}})} , \tag{49}$$

where $U_{\text{laser}}(\lambda_{\text{laser}} - \lambda_{\text{eff}})$ is the voltage delivered by the spectroradiometer viewing the laser source tuned to λ_{eff} and with intensity $I_0(\lambda_{\text{eff}})$:

$$I_0(\lambda_{\text{laser}}) = \int_0^\infty U_{\text{laser}}(\lambda_{\text{laser}} - \lambda_{\text{eff}}) d\lambda_{\text{eff}} . \tag{50}$$

With this definition, the slit scattering function of the spectroradiometer has a unit integral over optical wavelengths.

5.1.2.2 Optical responsivity

From the definition of the slit scattering function, one can express the optical responsivity, $R_{\text{opt}}(\lambda_{\text{laser}})$, of the spectroradiometer calibrated with the integrating sphere radiance at the laser wavelength:

$$R_{\text{opt}}(\lambda_{\text{laser}}) = \frac{I_0(\lambda_{\text{laser}})}{L_0(\lambda_{\text{laser}})} . \tag{51}$$

The optical responsivity of the spectroradiometer (see Figure 9) is then extrapolated to another wavelength λ using an ITS-90 fixed-point blackbody of known temperature (e.g., copper, at $T_{90} = 1357.77$ K):

$$R_{\text{opt}}(\lambda) = \frac{L_{\text{b}}(\lambda_{\text{laser}},T)}{L_{\text{b}}(\lambda,T)} \frac{U_{\text{b}}(\lambda,T)}{U_{\text{b}}(\lambda_{\text{laser}},T)} \frac{I_0(\lambda_{\text{laser}})}{L_0(\lambda_{\text{laser}})} . \tag{52}$$

The spectral responsivity of the spectroradiometer can be fully expressed from the measurement variables:

$$R(\lambda,\lambda_{\text{eff}}) = \frac{U_{\text{laser}}(\lambda - \lambda_{\text{eff}})}{L_0(\lambda_{\text{laser}})} \frac{L_{\text{b}}(\lambda_{\text{laser}},T)}{L_{\text{b}}(\lambda,T)} \frac{U_{\text{b}}(\lambda,T)}{U_{\text{b}}(\lambda_{\text{laser}},T)} . \tag{53}$$

This relative method used to calibrate the optical responsivity of the spectroradiometer is not critical as the determination of the thermodynamic temperature of the blackbody is performed at the laser wavelength. In these conditions, $R(\lambda_{\text{laser}},\lambda_{\text{laser}}) = U_{\text{laser}}(0)/L_0(\lambda_{\text{laser}})$.
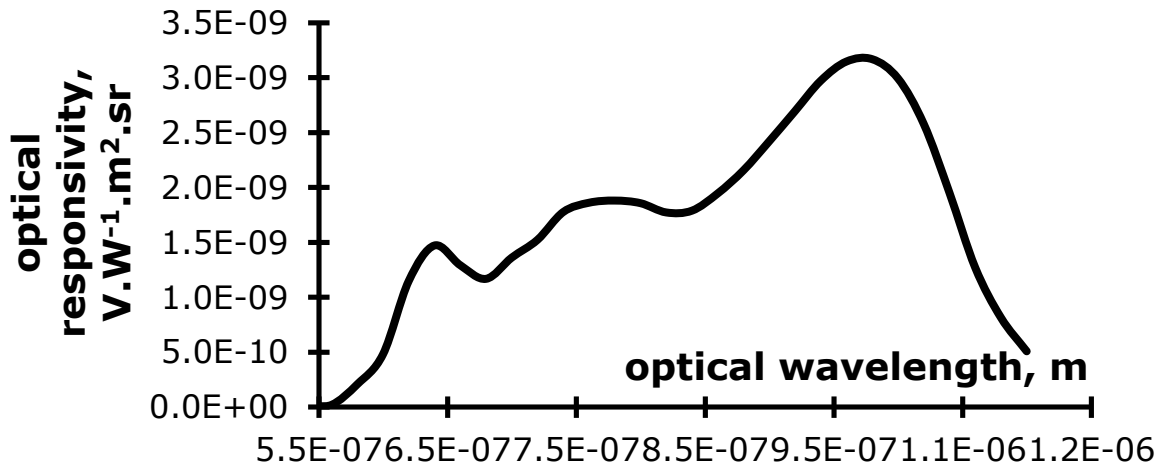
Figure 9. Optical responsivity of a spectroradiometer.

5.1.2.3 Out-of-band stray light

The Czerny Turner monochromator is subject to stray light outside its narrow detection bandwidth. While the optical diffusion level remains negligible (about a few parts in 10^6), its summation over the full visible spectrum range represents a non-negligible fraction (about one part in 10^3) of the detected optical power. The out-of-band stray light correction depends on the temperature, T, of the blackbody, and on the measurement wavelength, λ_{eff}, selected by the spectroradiometer. The out-of-band stray light can be defined as the signal coming from outside of the detection bandwidth used to compute the thermodynamic temperature. As the spectroradiometer spectral responsivity is recorded in a spectral bandwidth $[\lambda_{\text{eff}} - \delta\lambda, \lambda_{\text{eff}} + \delta\lambda]$, the signal part coming from outside of this spectral band must be corrected. The voltage $U_{\text{b}}(\lambda_{\text{eff}},T)$ delivered by the spectroradiometer viewing a blackbody is then composed of an in-band signal voltage $U_{\text{b}}^0(\lambda_{\text{eff}},T)$ and an out-of-band voltage $U_{\text{OOB}}(\lambda_{\text{eff}},T)$:

$$U_{\text{b}}(\lambda_{\text{eff}},T) = U_{\text{b}}^0(\lambda_{\text{eff}},T) + U_{\text{OOB}}(\lambda_{\text{eff}},T), \tag{54}$$

where

37

$$U_{\mathrm{b}}^{0}(\lambda_{\mathrm{eff}},T) = \int_{\lambda_{\mathrm{eff}}-\delta\lambda}^{\lambda_{\mathrm{eff}}+\delta\lambda} R(\lambda,\lambda_{\mathrm{eff}})L(\lambda,T)d\lambda$$

$$\approx L(\lambda_{\mathrm{eff}},T)\int_{\lambda_{\mathrm{eff}}-\delta\lambda}^{\lambda_{\mathrm{eff}}+\delta\lambda} R(\lambda,\lambda_{\mathrm{eff}})d\lambda \qquad (55)$$

and

$$U_{\mathrm{OOB}}(\lambda_{\mathrm{eff}},T) = \int_{0}^{\lambda_{\mathrm{eff}}-\delta\lambda} R(\lambda,\lambda_{\mathrm{eff}})L(\lambda,T)d\lambda + \int_{\lambda_{\mathrm{eff}}+\delta\lambda}^{\infty} R(\lambda,\lambda_{\mathrm{eff}})L(\lambda,T)d\lambda . \qquad (56)$$

The value of out-of-band stray light depends on the wavelength range, $\delta\lambda$, chosen for the computation of the thermodynamic temperature. Its measurement is performed with a continuous wave, fixed wavelength laser whose beam is injected into an integrating sphere to produce a quasi-Lambertian light distribution. As laser light is coherent, optical diffusion on the integrating sphere wall produces optical speckle that enhances detection noise. The speckle pattern is filtered by time-averaging after the laser beam passes through a multimode optical fibre that is agitated by an ultrasonic bath. This method is limited by a signal-to-noise ratio of about 10^5, while 10^6 is required. Repeating the recording and averaging of the slit scattering function over a whole day helps to lower the noise power by one order of magnitude. The computed out-of-band stray light correction is given in Table 7. The out-of-band correction factor (see Eq. (12)) is defined as:

$$K_{\mathrm{OOB}}(\lambda_{\mathrm{eff}},T) = 1 + \frac{U_{\mathrm{OOB}}(\lambda_{\mathrm{eff}},T)}{U_{\mathrm{b}}^{0}(\lambda_{\mathrm{eff}},T)} . \qquad (57)$$

Table 7. Temperature correction (expressed in kelvin) caused by out-of-band stray light with effective detection wavelength λ and blackbody temperature T.

$\lambda \setminus T$	1358 K	1500 K	2000 K	2750 K
730 nm	−0.127	−0.128	−0.164	−0.263
830 nm	−0.084	−0.098	−0.159	−0.289
910 nm	−0.071	−0.086	−0.150	−0.285

Table 8. Typical corrections and uncertainties related to the use of a monochromator-based spectroradiometer.

Component	Component value	Uncertainty value	Uncertainty unit	Sensitivity value	Sensitivity unit	Temperature uncertainty at the copper point (K)
λ_{eff}	8.000043×10^{-7}	1.0×10^{-11}	m	1.7×10^{9}	K.m^{-1}	0.017
Int(λ_{eff})	2.9215×10^{-8}	5.3×10^{-12}	V.W^{-1}.m^{3}.sr^{1}	3.5×10^{9}	K.V^{-1}.W.m^{-3}.sr^{-1}	0.018
K_{OOB}	1.0007	2.0×10^{-4}	no unit	105	K	0.021

6. Measurement of Sources

6.1 Sources of Uncertainty due to the Filter Radiometer

6.1.1 Size-of-source characteristic

The size-of-source effect (SSE) arises from scattering and diffraction of radiation and from aberrations within the optical/aperture system of a filter radiometer. This characteristic of the optical design of the filter radiometer causes some radiation from within the target area (nominal field-of-view) to be lost and some radiation from outside the nominal field-of-view to be detected. The filter radiometer signal will show a dependence on the size of the target (and on changes in the radiance distribution surrounding the target), hence the term 'size-of-source effect'. When using a calibrated filter radiometer, a correction needs to be applied to the measured signal, as typically the source under test and the source used in the calibration are not the same size and do not have the same surrounding spatial radiance distribution.

In order to quantify the size-of-source characteristic of a filter radiometer, the parameter $q_{\mathrm{SSE}}(r)$ is introduced [43], such that $q_{\mathrm{SSE}}(r)dr$ represents the fraction of radiation originating from an annulus of infinitesimal width dr, at a distance r from the centre of the field of view, that is scattered into the field-of-view. Three equivalent methods have been introduced to measure the size-of-source characteristic [43], each of which measures a slightly different quantity and is related to $q_{\mathrm{SSE}}(r)dr$ in a different way. These methods can be categorised as either direct or indirect methods [43, 44]. The direct method, which involves increasing the size of an aperture in front of a large uniform source, relies implicitly on the very high stability of that source. The indirect methods, which block the direct illumination within the instrument's field-of-view, are less sensitive to the stability of the source used.

For an instrument calibrated using the radiance method, the necessary correction depends on the difference in size (and radiance distribution) of the calibration source (the aperture on the integrating sphere) and the test source (the furnace and fixed-point or variable-temperature blackbody) and the size-of-source characteristic.

For an instrument calibrated using the hybrid method, the necessary correction depends on the absolute SSE [32]; i.e., the difference between the measured signal and that obtained from an infinitely large source, where the radiation scattered out of the field-of-view is balanced by light scattered into the field-of-view.

For an instrument calibrated with the irradiance or power method, the size-of-source characteristic is determined by the diffraction loss at the apertures. This is discussed in Section 4.1.7.

Filter radiometers and pyrometers can be designed to minimise the size-of-source characteristic [45], and size-of-source characteristics of $\sim 10^{-5}$ are achievable. This requires introducing a second, collimating lens after the second aperture and placing a baffle aperture, the so-called Lyot stop, in the collimated beam at a precise location.

In general, the size-of-source characteristic will be lower for an instrument designed for the radiance-method calibration than for an instrument designed for the hybrid-method calibration. The size-of-source characteristic can be reduced by selecting a lens with low scattering [46], and by using lenses that are anti-reflection coated. A high-quality achromatic lens, with minimal spherical aberration and

coma will also have a smaller size-of-source characteristic. It should be noted, however, that for the hybrid method, such lenses will need their transmittance calibrated at all wavelengths.

6.1.2 Size-of-source effect

The size-of-source effect (SSE) arises from the combination of the instrument size-of-source characteristic and the uniformity of the observed source.

The SSE correction [47], in its general form, is given by

$$S_{\text{cal}} = \left[1 + \sigma(R_{\text{eff,cal}}) - \sigma(R_{\text{eff,use}})\right] S,$$ (58)

where S_{cal} is the corrected signal, S is the measured signal and $\sigma(R)$ is the SSE quantity, related to $q_{\text{SSE}}(r)$, determined by any one of the direct or indirect methods available.

$R_{\text{eff,use}}$ is the effective radius of the target, and $R_{\text{eff,cal}}$ is the effective radius of the calibration target, which will be infinite for irradiance-method calibrations. The effective radius of a given source can be calculated using

$$\sigma(R_{\text{eff}}) = \sigma(R_0) + \frac{1}{S_0} \sum_{i=1}^{N} \left[\sigma(R_i) - \sigma(R_{i-1})\right] S_i,$$ (59)

where it is assumed that the surroundings of the source can be divided into N distinct adjacent annular isothermal regions with radii R_i, whose signals measured by the filter radiometer are S_i, and R_0 and S_0 are the radius and measured signal, respectively, of the isothermal region of which the target is a part. Inherent in Eqs (58) and (59) is an assumption that the SSE quantity σ is small (close to 0 for indirect methods or close to 1 for direct methods). Alternative correction equations, which depend on the particular SSE measurement method used, are available if this is not the case [47].

The uncertainty in $\sigma(R_{\text{eff}})$ can be calculated by propagating the uncertainties in $\sigma(R)$ and R through Eq. (59). This can be achieved by first fitting a function to the measured SSE data to approximate $\sigma(R)$. A wide range of appropriate functions can be found in [48], and the uncertainty in the fitted function, $u(\sigma(R))$, can be determined using the method in [49]. The uncertainty in $\sigma(R_{\text{eff}})$ is then given by:

$$u\left(\sigma(R_{\text{eff}})\right) = \frac{1}{S_0} \left\{ u^2(S_0)\left[\sigma(R_{\text{eff}}) - \sigma(R_0)\right]^2 + \sum_{i=1}^{N} u^2(S_i)\left[\sigma(R_i) - \sigma(R_{i-1})\right]^2 \right.$$

$$\left. + \sum_{i=0}^{N} \left(S_i - S_{i+1}\right)^2 \left[u^2\left(\sigma(R_i)\right) + \left(\left.\frac{\partial \sigma(R)}{\partial R}\right|_{R=R_i}\right)^2 u^2(R_i)\right] \right\}^{1/2},$$ (60)

where $S_{N+1} = 0$ by definition.

The size-of-source effect introduces a scaling factor to the measured signal. Rearranging Eq. (58) gives the scaling factor, K_{SSE}:

$$K_{SSE} = \frac{S}{S_{cal}} = \frac{1}{1 + \sigma(R_{eff,cal}) - \sigma(R_{eff,use})} \ . \tag{61}$$

The relative uncertainty associated with the radiance measured by the filter radiometer due to the SSE is equal to $u(K_{SSE})/K_{SSE}$. Normal and best relative uncertainties are 0.01 % and 0.002 %, respectively. Note that for the hybrid method, $R_{eff,cal} = \infty$; that it, the SSE characteristic must be measured out to a sufficient source diameter that it flattens off.

6.1.3 Linearity

Equation (13) for the output signal of a filter radiometer is only valid if the instrument, including the amplifier, responds linearly to input flux. Any departures from linearity should be corrected for by including the correction factor K_{lin} from Eq. (12).

Methods for measuring linearity are roughly divided into two groups – 'dual-aperture' and 'combinatorial' methods [50]. Dual-aperture methods compare the sum of two signals when two individual apertures are successively illuminated with the combined signal obtained when both apertures are simultaneously illuminated. The flux levels are progressively increased to cover the range of signals expected in use, and the measured non-linearity values accumulate with increasing flux. The most common dual-aperture method is a flux-doubling method, in which it is arranged that the two individual signals are approximately equal, and the signal levels progressively double until the highest signal level is reached. This method tends to produce fairly sparse data.

If the linearity factor in Eq. (12) is defined as a continuous function of the measured signal, $K_{lin} = 1/\eta(S_{meas})$, then the linearised measured signal is simply given by

$$S = \eta(S_{meas})S_{meas} \ . \tag{62}$$

The function $\eta(S_{meas})$ is determined from a number of discrete linearity values, η_i, which in turn are accumulated from a set of measured linearity values $\eta_{meas,i}$. For the flux-doubling method, it can be shown that after k doublings, the linearity value is given by [50]

$$\eta_k = \eta_0 \prod_{j=1}^{k} \eta_{meas,j} \ , \tag{63}$$

where η_0 is the linearity value at the lowest signal level. The value of η_0 can be arbitrarily set to 1 for the lowest signal measured during calibration of the filter radiometer. The values of η_k can be interpolated to generate the continuous function $\eta(S_{meas})$. Because the values of η_k accumulate according to Eq. (63), the uncertainties in their values are highly correlated. The uncertainties are given by [50]

41

$$u(\eta_j) = \left[u^2(\eta_{j-1}) + u^2(\eta_{\mathrm{meas},j}) \right]^{1/2} \ \text{for } j = 2 \text{ to } N,$$ (64)

where there are N discrete linearity measurements, and $u(\eta_0) = 0$ and $u(\eta_1) = u(\eta_{\mathrm{meas},1})$. The correlation coefficients, $r(\eta_j, \eta_k)$, between each of the uncertainty components are

$$r(\eta_j, \eta_k) \approx \begin{cases} (j/k)^{1/2} \ \text{for } j \leq k \\ (k/j)^{1/2} \ \text{for } j > k. \end{cases}$$ (65)

Combinatorial methods, on the other hand, use several filters and multiple paths to generate a large number of inter-related flux levels covering the expected range of signal values [51, 52]. Non-linearity values are determined directly by comparing the measured signals with a model of the ideal signals using least-squares fitting techniques with the filter transmittances as adjustable parameters:

$$\eta_j = \frac{S_{\mathrm{ideal}}(\phi_j)}{S_{\mathrm{meas},j}},$$ (66)

where ϕ_j is the flux level for the jth measurement. The η_j values can again be interpolated to obtain the continuous linearity function $\eta(S_{\mathrm{meas}})$.

6.1.4 Instrument temperature sensitivity (room temperature and heating from furnace)

As discussed in Section 5.1.1.1, filter radiometers are sensitive to their operating temperature and this sensitivity depends on the type of filter and the detector, as interference filters will react differently than glass filters to changes in temperature. FRs generally have some means of temperature stabilisation, but there will be some residual sensitivity. In [1], Boivin *et al.* determined the sensitivity of the spectral responsivity to changes in operating temperature for glass-filter-based FRs. By measuring the responsivity of the FR with the operating temperature of the integrated thermoelectric cooler set to 20 °C and then 40 °C, the temperature sensitivity was determined. The responsivity and change in responsivity with operating temperature is shown in Figure 10.

If the FR is used to determine the temperature of a blackbody, the change in responsivity of the FR with operating temperature will lead to a change in the measured blackbody temperature. Figure 11 shows the change in measured blackbody temperature for a 1 K change in FR operating temperature. With the thermoelectric system described in [1], temperature stability of 0.05 K is achievable.
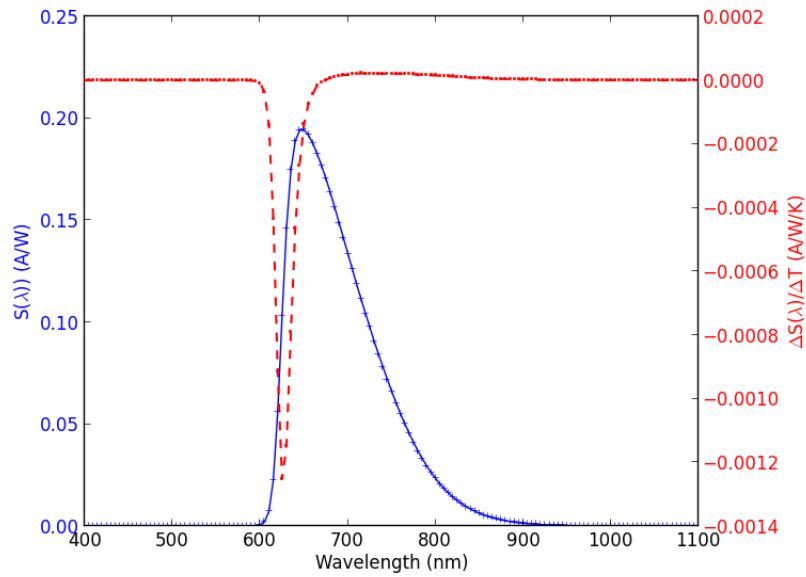
Figure 10. Responsivity (blue) and the change in responsivity with temperature (red) for a glass filter, Si detector filter radiometer with a central wavelength near 650 nm.
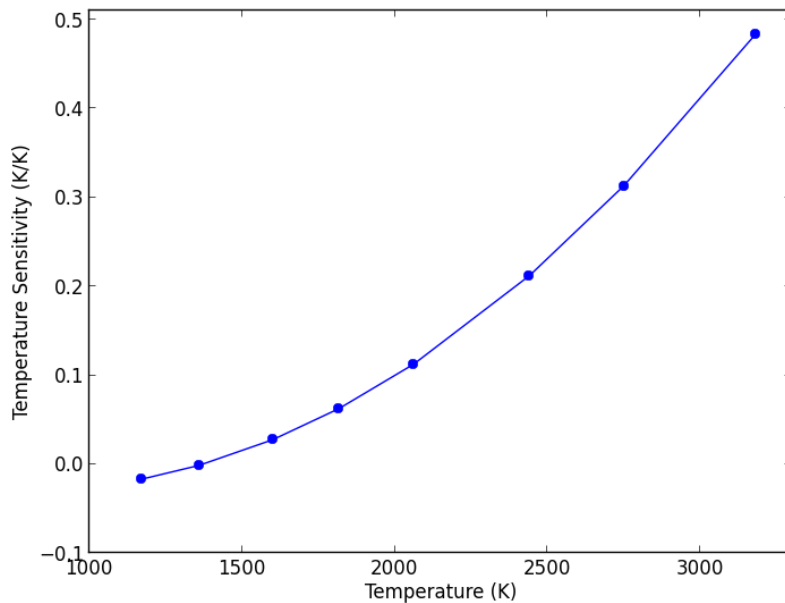
Figure 11. Change in the measured temperature (of a blackbody, for example) indicated by 650 nm, glass filter-based FR per degree of FR operating temperature change.

6.2 Sources of Uncertainty Due to the Source

6.2.1 Blackbody emissivity

The Monte-Carlo method is usually used for estimating a high-temperature blackbody's effective emissivity [53–55]. The uncertainty in the emissivity can by estimated using the same method by varying the cavity's surface reflectance and temperature distributions. Typical emissivities of large-area variable-temperature blackbodies in the visible are in the range from 0.999 to 0.9997 with a

standard uncertainty of 0.0002 to 0.0005 [56–58]. The typical emissivity of HTFPs is 0.9997 with a standard uncertainty of 0.0001 to 0.0002 [59, 60]. In the case of HTFP thermodynamic temperature measurement, the influence of the furnace cavity on the FP blackbody cavity must be taken into account [61].

The blackbody emissivity and the blackbody temperature measured with a filter radiometer are related by Eq. (12). However, for estimation of the temperature uncertainty component associated with the emissivity, we can assume that the filter radiometer spectral bandpass is narrow enough that the monochromatic approximation can be applied. For typical wavelengths and temperatures, the Wien approximation can also be applied. Therefore, the corresponding temperature uncertainty component arising from the emissivity uncertainty is given by

$$u_\varepsilon(T) = \frac{n\lambda_0 T^2}{c_2} u_{\text{rel}}(\varepsilon_{\text{BB}}),$$ (67)

where T and ε_{BB} are the temperature and effective emissivity, respectively, of the blackbody, and $u_{\text{rel}}(\varepsilon_{\text{BB}})$ is the relative uncertainty in the effective emissivity.

When using the irradiance method, a variable-temperature blackbody (VTBB) is used as an intermediator between an irradiance-mode filter radiometer and a radiation thermometer. The filter radiometer [62, 63] is used for measuring the thermodynamic temperature of the blackbody and then, immediately after that, the blackbody is used for calibration of the radiation thermometer, which later is used for HTFP radiance temperature measurement. In this case the emissivity of the VTBB must be taken into account. Applying the monochromatic and Wien approximations, the signals of the filter radiometer, S_{FR}, and the radiation thermometer, S_{RT}, can be expressed as

$$S_{\text{FR}} = R_{\text{eff,FR}} \varepsilon_{\text{BB}}(\lambda_{0,\text{FR}}) \frac{c_1}{n^2 \lambda_{0,\text{FR}}^5} \exp\left(-\frac{c_2}{n\lambda_{0,\text{FR}} T_{\text{VTBB}}}\right)$$ (68)

and

$$S_{\text{RT}} = R_{\text{eff,RT}} \varepsilon_{\text{BB}}(\lambda_{0,\text{RT}}) \frac{c_1}{n^2 \lambda_{0,\text{RT}}^5} \exp\left(-\frac{c_2}{n\lambda_{0,\text{RT}} T_{\text{VTBB}}}\right),$$ (69)

where $\lambda_{0,\text{FR}}$ and $\lambda_{0,\text{RT}}$ are the mean wavelengths of the filter radiometer and radiation thermometer, respectively, $R_{\text{eff,FR}}$ and $R_{\text{eff,RT}}$ are effective responsivity of the filter radiometer and radiation thermometer, $\varepsilon_{\text{BB}}(\lambda_{0,\text{FR}})$ and $\varepsilon_{\text{BB}}(\lambda_{0,\text{RT}})$ are the emissivities of VTBB at the mean wavelength of the filter radiometer and radiation thermometer, and T_{VTBB} is the temperature of the VTBB. Therefore, the thermometer signal, S_{RT}, is related to the filter radiometer signal, S_{FR}, by:

$$S_{\text{RT}} = S_{\text{RF}} \frac{R_{\text{eff,RT}}}{R_{\text{eff,FR}}} \frac{\varepsilon_{\text{BB}}(\lambda_{0,\text{RT}})}{\varepsilon_{\text{BB}}(\lambda_{0,\text{FR}})} \frac{\lambda_{0,\text{FR}}^5}{\lambda_{0,\text{RT}}^5} \exp\left(\frac{c_2}{n T_{\text{VTBB}}}\left(\frac{1}{\lambda_{0,\text{FR}}} - \frac{1}{\lambda_{0,\text{RT}}}\right)\right).$$ (70)

which is proportional to:

$$S_{\mathrm{RT}} \propto \frac{\varepsilon_{\mathrm{BB}}(\lambda_{0,\mathrm{RT}})}{\varepsilon_{\mathrm{BB}}(\lambda_{0,\mathrm{FR}})} = \left(1 + \frac{\Delta\varepsilon_{\mathrm{BB}}}{\varepsilon_{\mathrm{BB}}(\lambda_{0,\mathrm{FR}})}\right), \tag{71}$$

where $\Delta\varepsilon_{\mathrm{BB}}$ is the difference between the emissivities at the two wavelengths. Because $\varepsilon_{\mathrm{BB}}(\lambda_{0,FR})$ is very close to unity, Eq. (71) can be rewritten as

$$S_{\mathrm{RT}} \propto \left(1 + \Delta\varepsilon_{\mathrm{BB}}\right). \tag{72}$$

The radiance of the HTFP blackbody, $L_{\mathrm{HTFP}}(\lambda_{0,RT}, T_{\mathrm{HTFP}})$, will be proportional to the radiation thermometer signal when it's used for the HTFP measurement. Note that $T_{\mathrm{HTFP}} \approx T_{\mathrm{VTBB}}$, because the temperature of the VTBB is intentionally kept as close as possible to the temperature of the HTFP. Therefore,

$$L_{\mathrm{HTFP}}(\lambda_{0,RT}, T_{\mathrm{HTFP}}) \propto S_{\mathrm{RT}} \propto \left(1 + \Delta\varepsilon_{\mathrm{BB}}\right), \tag{73}$$

and the HTFP blackbody radiance uncertainty component associated with the emissivity of the VTBB equals the uncertainty in the difference between the VTBB emissivity at the mean wavelength of the filter radiometer and the VTBB emissivity at the mean wavelength of the radiation thermometer:

$$u_{\varepsilon_{\mathrm{BB}}}(L_{\mathrm{HTFP}}) = u(\Delta\varepsilon_{\mathrm{BB}}). \tag{74}$$

Filter radiometers and radiation thermometers are usually visible or near IR instruments. The emissivity of a VTBB in this spectral range does not depend strongly on wavelength and the variation is usually in the range 0.0001 to 0.0002. Therefore, the uncertainty $u(\Delta\varepsilon_{\mathrm{BB}})$ can be estimated as 0.0001 in the typical case, and even lower for the best case.

Therefore, the irradiance method, in comparison with the radiance and hybrid methods, has an additional uncertainty component related to the VTBB emissivity; however, this component is relatively small.

6.2.2 For variable temperature blackbodies

The stability and uniformity of a large-area variable-temperature blackbody (VTBB) must be taken into account when the irradiance (or power) method is applied for determining a HTPF's thermodynamic temperature; i.e., when an irradiance-mode filter radiometer (FR) is used for measuring the thermodynamic temperature of the VTBB and then a radiation thermometer (RT) is calibrated against the VTBB source.

6.2.2.1 VTBB stability

To minimise the effect of the VTBB instability, the FR and RT should measure the blackbody immediately after each other; i.e., the duration between the measurements with the FR and the RT should be as short as possible. Typically, a cycle of two measurements takes several minutes.

Two methods of VTBB stabilisation can be used: active, with optical feedback; and passive, with a constant blackbody electric current. Figure 12 shows typical stabilisation curves of the actively stabilised VNIIOFI-made blackbody BB3500MP. Stabilisation behaviour can change depending on the history of the blackbody (for instance, whether it was heated up or cooled down just before stabilisation). The usual instability characteristic is a monotonic drift. One can see that in the worst case, the drift has a rate of about 0.02 % (in terms of radiance at 650 nm) per 5 minutes, and the noise instability is less than 0.004 % (calculated as the standard deviation of 10 consecutive measurements). The passive stabilisation method features smaller noise but can suffer from unpredictable random change of the drift direction. To avoid this indeterminacy, it is recommended that a slight current ramp is applied, leading to a monotonic temperature drift. The best stability result [64] achieved with this technique is 0.2 K/h at a temperature of about 3000 K [65]; i.e., 0.05 % in terms of spectral radiance at 650 nm, which is comparable with the best results for the active method.

Assuming linear drift of the blackbody, the following measurement sequence is recommended: RT – FR – RT (or FR – RT – FR). In this case, the mean value of two RT measurements (before and after) corresponds to the FR measurement without any corrections for the blackbody stability. The difference $\Delta T_{\mathrm{RT}} = T_{\mathrm{RT,after}} - T_{\mathrm{RT,before}}$ between the blackbody temperature measured by the RT before and after the FR can be used for evaluating the upper limit of the uncertainty component associated with VTBB stability:

$$u_{\mathrm{VTBB,stab}} = \frac{\Delta T_{\mathrm{RT}}}{\sqrt{12}} \ . \tag{75}$$

During the WP5 (InK WP1) for HTFP temperature measurements at VNIIOFI, ΔT_{RT} varied from 0.01 K to 0.05 K. Therefore, the corresponding uncertainty component was typically within 0.01 K (0.009 % in terms of radiance at 650 nm at the temperature level corresponding to the Co-C point).
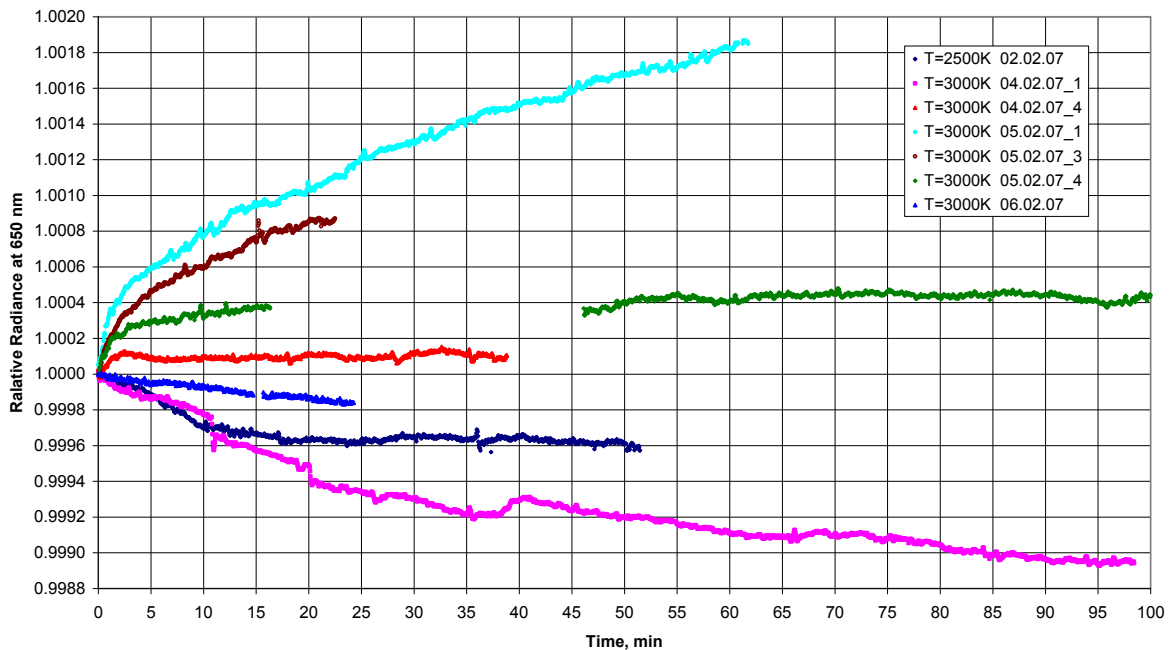
Figure 12. Typical stability of the actively stabilised VTBB of the BB3500 type.

6.2.2.2 VTBB uniformity

A VTBB is generally not perfectly uniform. The FR and RT may view different areas of the VTBB's cavity bottom. Therefore, the uncertainty component $u_{\text{VTBB,uniform}}$ (and maybe a correction factor) associated with the VTBB uniformity must be estimated. To minimise the correction and associated uncertainty, the blackbody must be as uniform as possible and the geometry of the measurements (diameters of apertures, RT optics, and measurement distances) must be chosen in such a way that both detectors (RT and FR) see as close as possible the same area of the cavity bottom. The uniformity should be measured and then used for an estimation of the uncertainty.

As an example, Figure 13 shows the uniformity, plotted as a radiance distribution along the cavity bottom in the horizontal direction, of the blackbody BB3500M used at VNIIOFI as the VTBB for WP5 (WP1 of InK). The FR had an aperture of 5 mm and was positioned at a distance of 720 mm from the blackbody aperture (BB aperture), whose diameter was 8 mm; the distance from the BB aperture to the blackbody bottom was 350 mm. The RT had an effective lens aperture of 34 mm and was focused at the BB aperture; the distance from the RT lens to the BB aperture was 750 mm. So, the FR and RT detectors saw at the BB bottom circular areas with diameters of about 14 mm and 16 mm, respectively; i.e., the RT saw a larger area. To check the influence of this difference, the RT was moved towards the BB aperture by about 40 mm without re-focusing, so it saw in this position an area of about 14 mm (similar to that of the FR). The difference between the RT temperature readings, $\Delta T_{\text{RT,un}}$, taken in the two RT positions was 0.04 K, 0.03 K, and less than 0.01 K for temperatures corresponding to the Co-C, Pt-C, and Re-C eutectic points, respectively. These values were applied as corrections, and the uncertainty component associated with the blackbody uniformity was estimated as 0.02 K for Co-C and Pt-C, and 0.01 K for Re-C, using an approximate relation:

$$u_{\text{VTBB,uniform}} = \frac{\Delta T_{\text{RT,un}}}{\sqrt{3}} . \qquad (76)$$

The experiment described above and Figure 13 show that the uniformity of 0.2 % within the observed area leads to reasonably low uncertainties in the case where both detectors (FR and RT) observe comparable areas of the cavity bottom.

The VTBB uniformity results presented in Figure 13 are comparable with that published elsewhere [66]. Therefore, based on the above example we can conclude that the normal uncertainty associated with VTBB uniformity is within 0.02 %, and for the best case is less than 0.01 %, in terms of radiance in the visible.
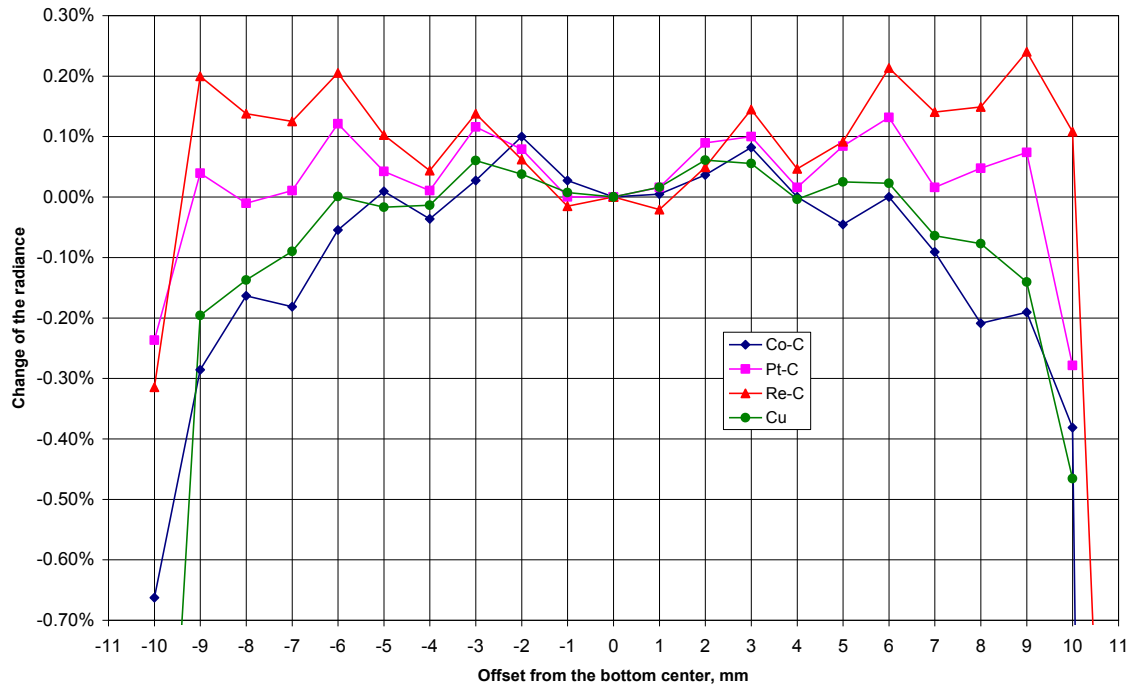
Figure 13. Cavity bottom uniformity of the blackbody BB3500M measured at VNIIOFI for Co-C, Pt-C, Re-C, and Cu points. The measurements were carried out at a wavelength of 900 nm for the Cu point, and 650 nm for the other three points.

6.2.3 For fixed-points

There are a number of effects related to pure-metal or eutectic fixed-points that lead to uncertainties in the measured temperatures of these fixed points. In addition to the uncertainty in effective emissivity discussed above, these include impurities, cavity-bottom temperature drop, and plateau identification. These uncertainties have been described for pure-metal fixed points in [67]. For the eutectic fixed-points additional uncertainties include structure effect, identification of the point of inflection or identification of the liquidus point, stability, furnace effect, and uncertainties of unknown origin. These are discussed in detail for Co-C, Pt-C, and Re-C in [68].

7. Example Uncertainty Budgets

7.1 Uncertainty Components for Each Calibration Scheme

Following the format of Figure 5, Table 9 lists all the uncertainty components and which calibration scheme they apply to.

Table 9. Uncertainty components required for each method – power, irradiance, hybrid, and radiance.

Uncertainty Component		Power	Irradiance	Hybrid	Radiance
Filter Radiometer Calibration					
Wavelength scale		✓	✓	✓	✓
Stray light in calibration		✓	✓	✓	✓
Responsivity of trap detector		✓	✓	✓	✓
Out-of-band effects		✓	✓	✓	✓
Amplification of photocurrent		✓	✓	✓	✓
Geometric factor	Distance	✓	✓	✓	✓
	FR aperture area	✓			
	Source aperture area	✓			✓
	Transfer/trap aperture area		✓	✓	✓
	Aperture co-alignment	✓	✓	✓	✓
	Aperture non-roundness	✓	✓	✓	✓
	Aperture change	✓	✓	✓	✓
Noise		✓	✓	✓	✓
FR spatial uniformity		✓			
Ageing and repeatability of trap detector		✓			
Temperature of trap detector		✓			
Diffraction		✓	✓		✓
Lens transmittance				✓	
Absolute SSE				✓	
Uniformity of irradiance field			✓	✓	
SSE					✓
Measurement of Blackbody					
Linearity		✓	✓	✓	✓
FR temperature stability		✓	✓	✓	✓
Effective emissivity of blackbody		✓	✓	✓	✓
Source uniformity		✓	✓	✓	✓
Source stability		✓	✓	✓	✓
Fixed point transition definition		✓	✓	✓	✓

7.2 Uncertainty Values

Tables 10 and 11 give values for each uncertainty component listed in Table 9, largely taken from the uncertainty budgets in the supplementary information for the work reported in [69]. These values are categorised as being "normal" and "best"; however, given the complexity of primary radiometry, even the "normal" uncertainties are not easily obtainable at any NMI.

Table 10. Typical contributions to the uncertainty budget for the calibration of a filter radiometer. All uncertainties are standard uncertainties.

Uncertainty Component		Normal Uncertainty	Best Uncertainty	Notes
Filter Radiometer Calibration				
Wavelength scale		100 pm	0.1 pm	Normal uncertainty for monochromator and best for laser system.
Stray light in calibration		0.01 %	0.0003 %	Based on the stray light values reported in [69].
Responsivity of trap detector		0.07 %	0.013 %	Absolute calibration traceable to a cryogenic radiometer.
Out-of-band effects		0.025 %	0.01 %	Based on the OOB values reported in [69].
Amplification of photocurrent		0.0026 %	0.001 %	
Geometric factor	Distance	0.1 %	0.004 %	All expressed as uncertainties in radiance, as per Table 3.
	FR aperture radius	0.02 %	0.01 %	
	Source aperture radius	0.02 %	0.01 %	
	Transfer/trap aperture radius	0.02 %	0.01 %	
	Aperture co-alignment	0.01 %	0.0001 %	
	Aperture non-roundness	0.004 %	0.001 %	
	Aperture change	0.02 %	0	
Noise		0.05%	0.01%	
FR spatial uniformity		0.02 %	0.02 %	Only for the power method since the FR is calibrated under-filled and used overfilled.
Ageing and repeatability of trap detector		0.03 %	0.01 %	0.01 % per year has been measured [41].
Temperature of trap detector		0.01 %	0.003 %	Based on the sensitivities reported in [69].
Diffraction		0.07 %	0.001 %	Diffraction at source/trap/FR depending on the method.
Lens transmittance		0.02 %	0.02 %	
Uniformity of irradiance field		0.03 %	0.013 %	
SSE		0.01 %	0.002 %	Based on the SSEs reported in [69].

Table 11. Typical contributions to the uncertainty budget for the measurement of a blackbody. All uncertainties are standard uncertainties.

Uncertainty Component	Normal Uncertainty	Best Uncertainty	Notes
Measurement of Blackbody			
Linearity	0.01 %	0.002 %	
FR temperature stability	0.01 %	0.002 %	
Effective emissivity of blackbody	0.008 %	0.008 %	
Source uniformity	0.02 %	0.01 %	For VTBB.
Source stability	0.12 %	0.03 %	For VTBB.
Fixed-point transition definition	See [67, 68]	See [67, 68]	

Figures 14 and 15 show plots of the propagated uncertainties for measurements of a variable-temperature blackbody over the range 1000 °C to 3000 °C for each of the four calibration schemes, for the normal and best uncertainties, respectively, based on the values given in Tables 10 and 11. These curves have been calculated assuming there are no correlations between any of the uncertainty components. There is little difference between each of the schemes.
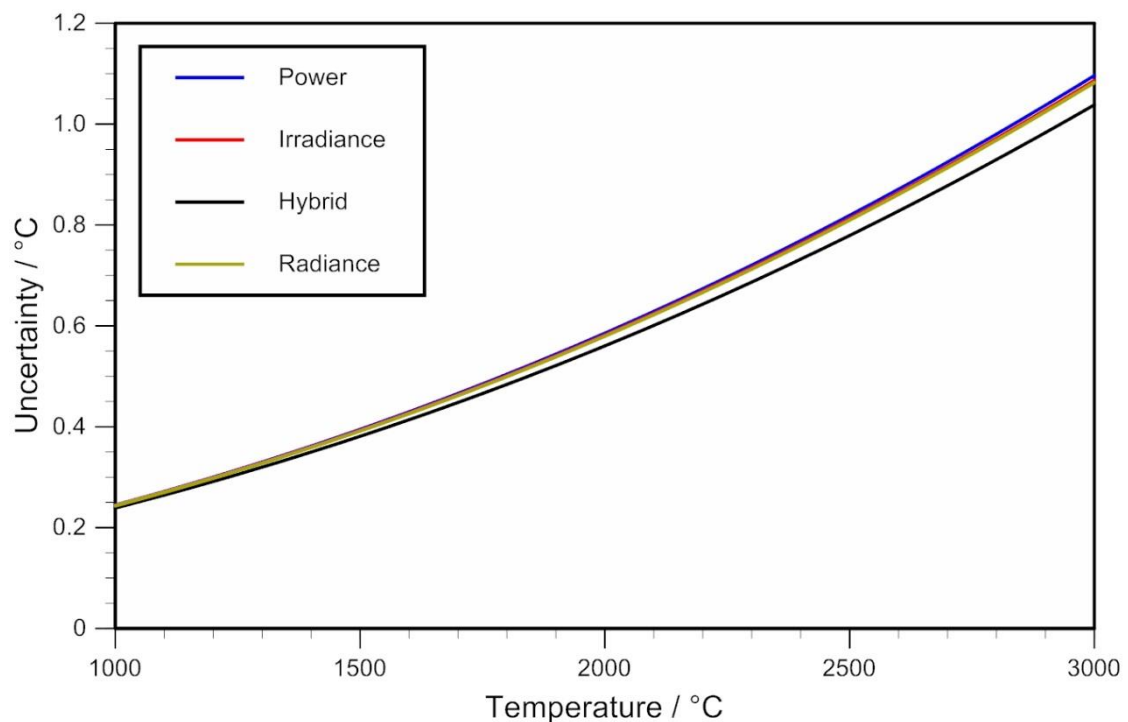
Figure 14. Uncertainties for each calibration scheme, propagated from the normal values given in Tables 10 and 11.
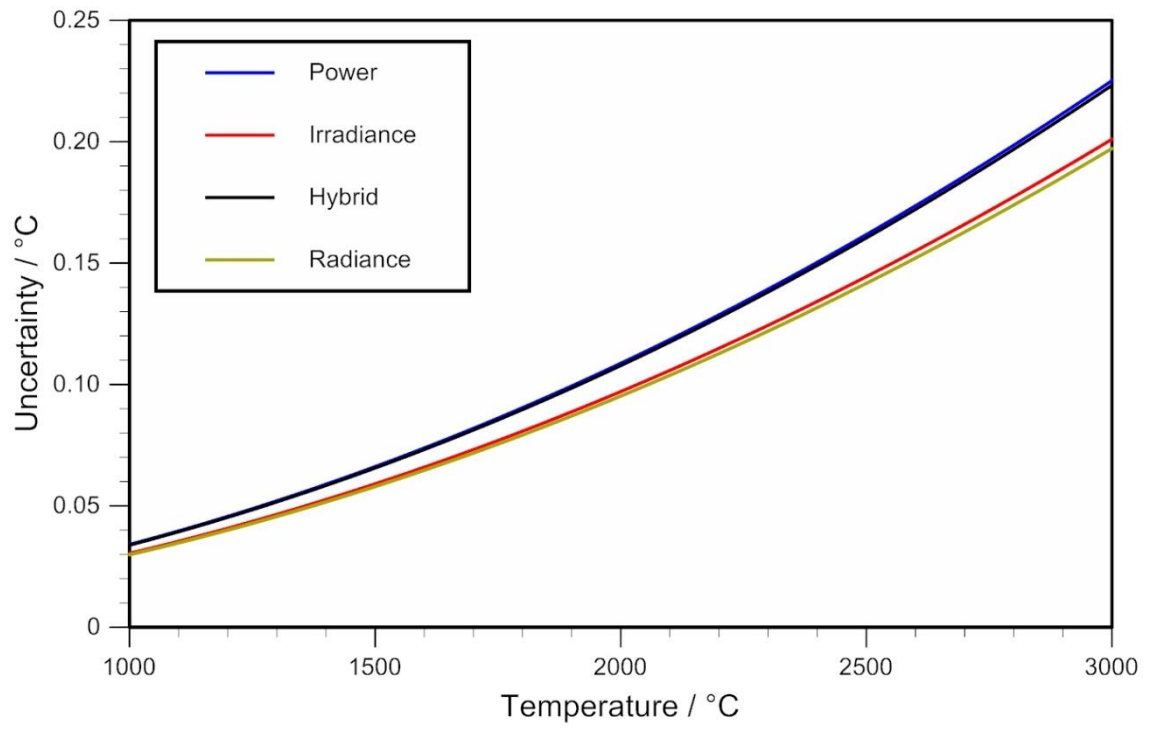
Figure 15. Uncertainties for each calibration scheme, propagated from the best values given in Tables 10 and 11.

Appendix A. Uncertainty Propagation Based on the Integral

A.1 Concepts

The method of propagating uncertainties directly through the integral in Eq. (13) is described in detail in [70] and has also been published in [57, 71, 72]. This method calculates the sensitivity coefficients in terms of signal directly from the practical numerical implementation of Eq. (13), and uses implicit differentiation to convert these into sensitivity coefficients in terms of temperature.

In practice, Eq. (13) is solved by introducing the numerical summation (trapezium rule):

$$S = \frac{K}{2}\left[s_1 L_b(\lambda_1,T)(\lambda_2 - \lambda_1) + \sum_{i=2}^{N-1} s_i L_b(\lambda_i,T)(\lambda_{i+1} - \lambda_{i-1}) + s_N L_b(\lambda_N,T)(\lambda_N - \lambda_{N-1}) \right]$$
$$= \frac{K}{2}\sum_{i=1}^{N} s_i L_b(\lambda_i,T)\delta\lambda_i \ , \tag{77}$$

where the spectral responsivity has been sampled at N wavelengths (not necessarily at equal wavelength intervals) with measured wavelength–spectral responsivity pairs (λ_i, s_i), and

$$\delta\lambda_i = \begin{cases} \lambda_2 - \lambda_1 & \text{if } i = 1 \\ \lambda_{i+1} - \lambda_{i-1} & \text{if } 1 < i < N \\ \lambda_N - \lambda_{N-1} & \text{if } i = N. \end{cases} \tag{78}$$

For a given measured value of S, the value of T is determined iteratively by repeatedly evaluating the right-hand side of Eq. (77) with different trial values of T until the right-hand side is equal to S. The most efficient method of doing this is to use the Newton-Raphson algorithm as given by Eq. (14) and outlined in [8].

Regardless of the algorithm used to solve Eq. (77) for T, the *uncertainty* in the value of T can be determined directly from Eq. (77) as a function of the uncertainties in the measured (λ_i, s_i) values and the uncertainties in K and S. In order to calculate the appropriate sensitivity coefficients, it will be assumed that the errors in the measurements can be separated into purely random components (that is, components that vary independently from measurement to measurement; e.g., measurement noise) and purely systematic components (that is, fully correlated components that are constant from one measurement to the next; e.g., uniformity of reference source, alignment, wavelength scale offset). (Partially correlated components will not be considered explicitly, but can easily be accommodated using the sensitivity coefficients derived below.) Thus, the wavelength and responsivity measurements can be modelled as:

$$\lambda_i = \lambda_{\text{true},i} + \lambda_{\text{ran},i} + \lambda_{\text{sys}} \tag{79}$$

and

$$s_i = s_{\text{true},i}(1 + s_{\text{ran},i} + s_{\text{sys}}) , \tag{80}$$

where $\lambda_{\text{true},i}$ and $s_{\text{true},i}$ are the unknown true values of the ith wavelength and i^{th} responsivity, respectively, $\lambda_{\text{ran},i}$ is the unknown random error in the ith wavelength, λ_{sys} is the unknown systematic

error common to all wavelengths, $s_{\mathrm{ran},i}$ is the unknown random error in the ith responsivity, and s_{sys} is the unknown systematic error common to all responsivity measurements. Note that the wavelength errors are expressed as absolute values, while the responsivity errors are relative values. All of these errors have expectation values of zero, and are characterised by uncertainties $u(\lambda_{\mathrm{ran},i})$, $u(\lambda_{\mathrm{sys}})$, $u_{\mathrm{rel}}(s_{\mathrm{ran},i})$, and $u_{\mathrm{rel}}(s_{\mathrm{sys}})$, respectively. Thus, the expectation value of $\lambda_{\mathrm{true},i}$ is λ_i and the expectation value of $s_{\mathrm{true},i}$ is s_i. There is no need to separate the uncertainties in K and S into random and systematic components since the sensitivity coefficients for the random and systematic errors are the same as each other. Thus, there will be single combined uncertainties $u(K)$ and $u(S)$.

Substituting Eqs (79) and (80) into Eqs (77) and (78) and differentiating with respect to each of $\lambda_{\mathrm{ran},i}$, λ_{sys}, $s_{\mathrm{ran},i}$, s_{sys}, K, and T gives:

$$
\frac{\partial S}{\partial \lambda_{\mathrm{ran},i}} = \frac{K}{2}
\begin{cases}
s_1 \left.\dfrac{\partial L_{\mathrm{b}}(\lambda,T)}{\partial \lambda}\right|_{\lambda=\lambda_1} \delta\lambda_1 - s_1 L_{\mathrm{b}}(\lambda_1,T) - s_2 L_{\mathrm{b}}(\lambda_2,T) & \text{if } i=1 \\[2ex]
s_i \left.\dfrac{\partial L_{\mathrm{b}}(\lambda,T)}{\partial \lambda}\right|_{\lambda=\lambda_i} \delta\lambda_i + s_{i-1} L_{\mathrm{b}}(\lambda_{i-1},T) - s_{i+1} L_{\mathrm{b}}(\lambda_{i+1},T) & \text{if } 1<i<N \\[2ex]
s_N \left.\dfrac{\partial L_{\mathrm{b}}(\lambda,T)}{\partial \lambda}\right|_{\lambda=\lambda_N} \delta\lambda_N + s_{N-1} L_{\mathrm{b}}(\lambda_{N-1},T) + s_N L_{\mathrm{b}}(\lambda_N,T) & \text{if } i=N,
\end{cases}
\tag{81}
$$

$$
\frac{\partial S}{\partial \lambda_{\mathrm{sys}}} = \frac{K}{2} \sum_{i=1}^{N} s_i \left.\frac{\partial L_{\mathrm{b}}(\lambda,T)}{\partial \lambda}\right|_{\lambda=\lambda_i} \delta\lambda_i \ ,
\tag{82}
$$

$$
\frac{\partial S}{\partial s_{\mathrm{ran},i}} = \frac{K}{2} s_i L_{\mathrm{b}}(\lambda_i,T)\delta\lambda_i \ ,
\tag{83}
$$

$$
\frac{\partial S}{\partial s_{\mathrm{sys}}} = S \ ,
\tag{84}
$$

$$
\frac{\partial S}{\partial K} = \frac{S}{K} \ ,
\tag{85}
$$

and

$$
\frac{\partial S}{\partial T} = \frac{K}{2} \sum_{i=1}^{N} s_i \left.\frac{\partial L_{\mathrm{b}}(\lambda,T)}{\partial T}\right|_{\lambda=\lambda_i} \delta\lambda_i
\tag{86}
$$

where

$$
\begin{aligned}
\left.\frac{\partial L_{\mathrm{b}}(\lambda,T)}{\partial \lambda}\right|_{\lambda=\lambda_i} &= \frac{L_{\mathrm{b}}(\lambda_i,T)}{\lambda_i}\left[\frac{c_2}{n\lambda_i T\left[1-\exp\left(-c_2/(n\lambda_i T)\right)\right]} - 5 \right] \\[2ex]
&\approx \frac{L_{\mathrm{b}}(\lambda_i,T)}{\lambda_i}\left[\frac{c_2}{n\lambda_i T} - 5 \right] \text{ (Wien approximation)}
\end{aligned}
\tag{87}
$$

and

$$\frac{\partial L_{\text{b}}(\lambda,T)}{\partial T}\bigg|_{\lambda=\lambda_i} = \frac{c_2}{n\lambda_i T^2\left[1-\exp\left(-c_2/(n\lambda_i T)\right)\right]}L_{\text{b}}(\lambda_i,T)$$
$$\approx \frac{c_2}{n\lambda_i T^2}L_{\text{b}}(\lambda_i,T) \text{ (Wien approximation)}. \tag{88}$$

The sensitivity coefficients for temperature are obtained by applying the rule for implicit differentiation:

$$\frac{\partial T}{\partial \lambda_{\text{ran},i}} = -\frac{\partial S}{\partial \lambda_{\text{ran},i}}\bigg/\frac{\partial S}{\partial T}, \tag{89}$$

$$\frac{\partial T}{\partial \lambda_{\text{sys}}} = -\frac{\partial S}{\partial \lambda_{\text{sys}}}\bigg/\frac{\partial S}{\partial T}, \tag{90}$$

$$\frac{\partial T}{\partial s_{\text{ran},i}} = -\frac{\partial S}{\partial s_{\text{ran},i}}\bigg/\frac{\partial S}{\partial T}, \tag{91}$$

$$\frac{\partial T}{\partial s_{\text{sys}}} = -\frac{\partial S}{\partial s_{\text{sys}}}\bigg/\frac{\partial S}{\partial T}, \tag{92}$$

$$\frac{\partial T}{\partial K} = -\frac{\partial S}{\partial K}\bigg/\frac{\partial S}{\partial T}, \tag{93}$$

$$\frac{\partial T}{\partial S} = \frac{1}{\partial S/\partial T}. \tag{94}$$

The uncertainty in temperature is given by the GUM law for propagation of uncertainty as

$$u^2(T) = \sum_{i=1}^{N}\left[\left(\frac{\partial T}{\partial \lambda_{\text{ran},i}}u(\lambda_{\text{ran},i})\right)^2 + \left(\frac{\partial T}{\partial s_{\text{ran},i}}u_{\text{rel}}(s_{\text{ran},i})\right)^2\right]$$
$$+ \left(\frac{\partial T}{\partial \lambda_{\text{sys}}}u(\lambda_{\text{sys}})\right)^2 + \left(\frac{\partial T}{\partial s_{\text{sys}}}u_{\text{rel}}(s_{\text{sys}})\right)^2 + \left(\frac{\partial T}{\partial K}u(K)\right)^2 + \left(\frac{\partial T}{\partial S}u(S)\right)^2 \tag{95}$$

with the addition of any correlated components. For example, the uncertainties $u(K)$ and $u(S)$ may be partially correlated.

A.2 GUM Tree Calculator (GTC)

While the equations in Appendix A.1 look fearsome, with care they can be easily implemented in a software language of choice or in a spreadsheet application. Alternatively, a powerful technique, known as GUM Tree Calculator (GTC), which can automatically propagate uncertainties through any equation or series of inter-related equations, can be used. GTC can also propagate uncertainties through iterative algorithms, such as the Newton-Raphson algorithm. GTC is described in [73] and is available for download from the MSL website [74]. GTC can be used as an interactive calculator, or as a batch processing tool. It is self-contained (requiring no supporting software) and programmable using the Python language.

GTC uses a special data type, called an uncertain number, to represent quantities that have been measured, or estimated in some way. They are the key feature of GTC that distinguishes it from other data processing tools. An uncertain number in GTC is a variable data structure containing a value, a standard uncertainty, and a number of degrees of freedom. Correlation coefficients for any two uncertain numbers can also be assigned. Thus, when propagating uncertainties through Eq. (77), each of the λ_i and s_i measurements are treated as uncertain numbers with both random and systematic uncertainty components. When using Python, for example, coding of Eq. (77) is carried out with these uncertain-number variables in the same way that the integral would be coded using normal single-value variables. Then the Newton-Raphson algorithm (or any other suitable algorithm) can be applied, using the same uncertain-number variables, to determine the value of T. GTC automatically propagates the uncertainties through these calculations, using the method of automatic differentiation, which uses the chain rule of calculus, to implement the GUM propagation law. GTC will deliver a value, standard uncertainty, and number of degrees of freedom for T, and also provide a complete uncertainty budget if required.

A.3 How to Apply the Method for Different Sources of Uncertainty

This method is applied by calculating the sensitivity coefficients in Eqs (89) to (94) and combining the uncertainty components using Eq. (95). The appropriate sensitivity coefficients for common sources of uncertainty are calculated as follows.

Effect	Notes	Calculation
Spectral responsivity of trap detector, s_{trap}	If spectral in $s(\lambda)$, possibly affects all of $u(\lambda_{\text{ran},i})$, $u(\lambda_{\text{sys}})$, $u_{\text{rel}}(s_{\text{ran},i})$, and $u_{\text{rel}}(s_{\text{sys}})$. Otherwise in K.	Eqs (89) to (92) or $$\frac{\partial T}{\partial s_{\text{trap}}} = \frac{\partial K}{\partial s_{\text{trap}}} \frac{\partial T}{\partial K}$$ $$\frac{\partial K}{\partial \tau_{\text{trap}}} = \frac{K}{\tau_{\text{trap}}}$$ $\dfrac{\partial T}{\partial K}$ from Eq. (93).
Geometric factor, g	Uncertainty associated with geometric factor given by Eqs (24) and (28). Then in K.	$$\frac{\partial K}{\partial g} = \frac{K}{g}$$ $\dfrac{\partial T}{\partial K}$ from Eq. (93).
Amplifier gain, G	In K.	$$\frac{\partial K}{\partial G} = \frac{K}{G}$$ $\dfrac{\partial T}{\partial K}$ from Eq. (93).
Wavelength scale accuracy	This produces uncertainty components $u(\lambda_{\text{ran},i})$ and $u(\lambda_{\text{sys}})$. However, if the accuracy can be considered a spectral offset, it can be considered a simple uncertainty component $u(\lambda_{\text{sys}})$ only.	Eqs (89) and (90).

Filter stability	This will affect the shape of $s(\lambda)$ and hence possibly all of $u(\lambda_{\text{ran},i})$, $u(\lambda_{\text{sys}})$, $u_{\text{rel}}(s_{\text{ran},i})$, and $u_{\text{rel}}(s_{\text{sys}})$.	Eqs (89) to (92).
Instrument stability and noise	This affects the measured signal, S.	Eq. (94).
Size-of source effect, K_{SSE}	In K.	$\dfrac{\partial K}{\partial K_{\text{SSE}}} = \dfrac{K}{K_{\text{SSE}}}$ $\dfrac{\partial T}{\partial K}$ from Eq. (93).
Linearity, K_{lin}	In K.	$\dfrac{\partial K}{\partial K_{\text{lin}}} = \dfrac{K}{K_{\text{lin}}}$ $\dfrac{\partial T}{\partial K}$ from Eq. (93).
Blackbody emissivity, ε	In S when measuring a blackbody at an unknown temperature.	$\dfrac{\partial T}{\partial \varepsilon} = \dfrac{\partial S}{\partial \varepsilon}\dfrac{\partial T}{\partial S}$ $\dfrac{\partial S}{\partial \varepsilon} = \dfrac{S}{\varepsilon}$ $\dfrac{\partial T}{\partial S}$ from Eq. (94).
Blackbody stability, ability to define melt and similar	As above.	
Hybrid method: lens transmittance	If spectral in $s(\lambda)$, possibly affects all of $u(\lambda_{\text{ran},i})$, $u(\lambda_{\text{sys}})$, $u_{\text{rel}}(s_{\text{ran},i})$, and $u_{\text{rel}}(s_{\text{sys}})$. But normally K.	Eqs (87) to (92) or $\dfrac{\partial T}{\partial \tau_{\text{abs}}} = \dfrac{\partial K}{\partial \tau_{\text{abs}}}\dfrac{\partial T}{\partial K}$ $\dfrac{\partial K}{\partial \tau_{\text{abs}}} = \dfrac{K}{\tau_{\text{abs}}}$ $\dfrac{\partial T}{\partial K}$ from Eq. (93).
Power method: uniformity of detector	These can all be considered as a relative uncertainty within K.	$\dfrac{\partial T}{\partial K}$ from Eq. (93).
Radiance method: angular uniformity of the calibration source		
Irradiance/hybrid method: spatial uniformity of the calibration irradiance field		

Appendix B. Uncertainty Propagation Based on Key Spectral Parameters

B.1 Concepts

An alternative method of propagating the uncertainties in the spectral responsivity measurements to the measured temperature redefines the integral in Eq. (13) in terms of key spectral parameters of the filter radiometer. This method is most fully described in [75].

For the purpose of calculating temperature and its uncertainty, the measurement equation, Eq. (13), can be approximated by the Planck version of the Sakuma–Hattori equation [76]:

$$S(T) = \frac{C}{\exp\left(\dfrac{c_2}{AT + B}\right) - 1}, \tag{96}$$

where A, B, and C are parameters related to the optical properties of the filter radiometer. This approximation is valid for small[3] values of the relative bandwidth, $r = \sigma/\lambda_0$, of the spectral responsivity [77]. In this case [78]

$$A = n\lambda_0(1 - 6r^2), \tag{97}$$

$$B = \frac{c_2}{2}r^2, \tag{98}$$

$$C = K\frac{c_1}{n^2\lambda_0^5}(1 + 15r^2)\int_0^\infty s(\lambda)d\lambda = \frac{H}{n^2\lambda_0^5}(1 + 15r^2), \tag{99}$$

where λ_0 and σ are the mean wavelength and standard deviation (which is a measure of the bandwidth), respectively, of the spectral responsivity (as measured in air), n is the refractive index of air, and K (as described in Section 2.5) includes any optical, geometrical, and electrical quantities not included in $s(\lambda)$.

An advantage of using the approximation given by equation (96) is that it can be rearranged to give T directly as a function of S:

$$T = \frac{c_2}{A\ln\left(\dfrac{C}{S} + 1\right)} - \frac{B}{A}, \tag{100}$$

so that once A, B, and C have been calculated from H, λ_0, and σ, Eq. (100) can be used to calculate the temperature directly from subsequent measurements of S.

---

[3] The approximation, when the relative bandwidth is less than 0.01, e.g., for a 650 nm filter radiometer with bandwidth (full-width at half maximum) less than about 20 nm, typically creates an error smaller than 3 mK over the temperature range 600 °C to 3000 °C.

The values of H, λ_0, and σ can be calculated from $s(\lambda)$ through the following integrals [78]:

$$H = Kc_1 \int_0^\infty s(\lambda)d\lambda , \tag{101}$$

$$\lambda_0 = \frac{\int_0^\infty \lambda s(\lambda)d\lambda}{\int_0^\infty s(\lambda)d\lambda} , \tag{102}$$

$$\sigma^2 = \frac{\int_0^\infty (\lambda - \lambda_0)^2 s(\lambda)d\lambda}{\int_0^\infty s(\lambda)d\lambda} . \tag{103}$$

Equations (96) to (99) and (101) to (103) form the basis of the uncertainty analysis. Uncertainties in the values of H, λ_0, and σ, and additionally n and c_2, can be propagated through Eq. (96) using the following sensitivity coefficients:

$$\frac{\partial T}{\partial H} = -\frac{\partial S}{\partial H} \bigg/ \frac{\partial S}{\partial T} \approx -\frac{n\lambda_0 T^2 P}{c_2}\frac{1}{H} , \tag{104}$$

$$\frac{\partial T}{\partial \lambda_0} = -\frac{\partial S}{\partial \lambda_0} \bigg/ \frac{\partial S}{\partial T} \approx \frac{T}{\lambda_0}\left(5\frac{n\lambda_0 TP}{c_2} - 1\right) , \tag{105}$$

$$\frac{\partial T}{\partial \sigma} = -\frac{\partial S}{\partial \sigma} \bigg/ \frac{\partial S}{\partial T} \approx -\left(\frac{30nT^2 P}{c_2} - \frac{12T}{\lambda_0} + \frac{c_2}{n\lambda_0^2}\right)\frac{\sigma}{\lambda_0} , \tag{106}$$

$$\frac{\partial T}{\partial n} = -\frac{\partial S}{\partial n} \bigg/ \frac{\partial S}{\partial T} \approx \frac{T}{n}\left(2\frac{n\lambda_0 TP}{c_2} - 1\right) , \tag{107}$$

$$\frac{\partial T}{\partial c_2} = -\frac{\partial S}{\partial c_2} \bigg/ \frac{\partial S}{\partial T} = \frac{T}{c_2} , \tag{108}$$

where

$$P = 1 - \exp\left(\frac{-c_2}{n\lambda_0 T}\right) . \tag{109}$$

All of these components are determined during the calibration of the filter radiometer. Additionally, the uncertainty in measuring S during use when determining the unknown temperature is propagated to T by the sensitivity coefficient

$$\frac{\partial T}{\partial S} = \frac{1}{\partial S / \partial T} \approx \frac{n \lambda_0 T^2 P}{c_2} \frac{1}{S} .$$ (110)

The approximations indicated by the $\approx$ symbol in Eqs (104) to (107) and Eq. (110) arise from neglecting terms in the derivatives of order r^2 or higher (narrowband approximation). Additionally, the Wien approximation can be applied by replacing P with 1.

Each of the uncertainty components discussed in the main text can be identified with one of the six sensitivity coefficients of Eqs (104) to (108) or Eq. (110), and contribute towards one of the uncertainty values $u(\lambda_0)$, $u(\sigma)$, $u(H)$, $u(n)$, $u(c_2)$, or $u(S)$. The total standard uncertainty in the calculated value of T is evaluated from the GUM formula:

$$u^2(T) = \left(\frac{\partial T}{\partial \lambda_0} u(\lambda_0) \right)^2 + \left(\frac{\partial T}{\partial \sigma} u(\sigma) \right)^2 + \left(\frac{\partial T}{\partial H} u(H) \right)^2 + \left(\frac{\partial T}{\partial n} u(n) \right)^2 + \left(\frac{\partial T}{\partial c_2} u(c_2) \right)^2 + \left(\frac{\partial T}{\partial S} u(S) \right)^2$$ (111)

with the addition of any correlated components. The narrowband and Wien approximations indicated above introduce insignificant error (typically less than 3 mK) into the calculated value of the total standard uncertainty for realistic values of the parameters. Because the uncertainties $u(n)$ and $u(c_2)$ are small, the fourth and fifth terms in Eq. (111) are negligible and can be removed from the equation. In fact, after the redefinition of the SI in 2019, $u(c_2)$ will be identically zero, since $c_2 = hc/k$ and h, c, and k will all have defined values. Similarly, the component of uncertainty in H due to c_1 is also negligible, and will be identically zero after the redefinition since $c_1 = 2hc^2$.

The uncertainties $u(H)$, $u(\lambda_0)$, and $u(\sigma)$ can be derived from the uncertainties $u(\lambda_{\mathrm{ran},i})$, $u(\lambda_{\mathrm{sys}})$, $u_{\mathrm{rel}}(s_{\mathrm{ran},i})$, $u_{\mathrm{rel}}(s_{\mathrm{sys}})$, and $u(K)$ in a similar fashion to the method in Appendix A. That is, each of the integrals in Eqs (101) to (103) can be expressed as numerical summations (given by the trapezium rule) in terms of the measured (λ_i, s_i) pairs, and the appropriate sensitivity coefficients calculated.

The sensitivity coefficients for H are:

$$\frac{\partial H}{\partial \lambda_{\mathrm{ran},i}} = \frac{K c_1}{2} \begin{cases} -s_1 - s_2 & \text{if } i = 1 \\ s_{i-1} - s_{i+1} & \text{if } 1 < i < N \\ s_{N-1} + s_N & \text{if } i = N, \end{cases}$$ (112)

$$\frac{\partial H}{\partial \lambda_{\mathrm{sys}}} = 0 ,$$ (113)

$$\frac{\partial H}{\partial s_{\mathrm{ran},i}} = \frac{K c_1}{2} s_i \delta \lambda_i ,$$ (114)

$$\frac{\partial H}{\partial s_{\text{sys}}} = H , \qquad (115)$$

and

$$\frac{\partial H}{\partial K} = \frac{H}{K} , \qquad (116)$$

where $\delta\lambda_i$ is given by Eq. (78) in Appendix A. The uncertainty $u(H)$ is then obtained from:

$$u^2(H) = \sum_{i=1}^{N} \left[\left(\frac{\partial H}{\partial \lambda_{\text{ran},i}} u(\lambda_{\text{ran},i}) \right)^2 + \left(\frac{\partial H}{\partial s_{\text{ran},i}} u_{\text{rel}}(s_{\text{ran},i}) \right)^2 \right] + H^2 u_{\text{rel}}^2(s_{\text{sys}}) + H^2 u_{\text{rel}}^2(K) . \qquad (117)$$

The sensitivity coefficients for λ_0 are:

$$\frac{\partial \lambda_0}{\partial \lambda_{\text{ran},i}} = \frac{Kc_1}{2H} \begin{cases} s_1\delta\lambda_1 - s_1(\lambda_1 - \lambda_0) - s_2(\lambda_2 - \lambda_0) & \text{if } i = 1 \\ s_i\delta\lambda_i + s_{i-1}(\lambda_{i-1} - \lambda_0) - s_{i+1}(\lambda_{i+1} - \lambda_0) & \text{if } 1 < i < N \\ s_N\delta\lambda_N + s_{N-1}(\lambda_{N-1} - \lambda_0) + s_N(\lambda_N - \lambda_0) & \text{if } i = N, \end{cases} \qquad (118)$$

$$\frac{\partial \lambda_0}{\partial \lambda_{\text{sys}}} = 1 , \qquad (119)$$

$$\frac{\partial \lambda_0}{\partial s_{\text{ran},i}} = \frac{Kc_1 s_i \delta\lambda_i}{2H}(\lambda_i - \lambda_0) , \qquad (120)$$

and

$$\frac{\partial \lambda_0}{\partial s_{\text{sys}}} = 0 . \qquad (121)$$

Note that in Eqs (118) and (120) $Kc_1/H = \left[\int_0^\infty s(\lambda)d\lambda \right]^{-1}$, the inverse of the area under the spectral responsivity curve (i.e., $\partial\lambda_0/\partial\lambda_{\text{ran},i}$ and $\partial\lambda_0/\partial s_{\text{ran},i}$ are independent of K and c_1, as expected from Eqs (102) and (103)). The uncertainty $u(\lambda_0)$ is then obtained from:

$$u^2(\lambda_0) = \sum_{i=1}^{N} \left[\left(\frac{\partial \lambda_0}{\partial \lambda_{\text{ran},i}} u(\lambda_{\text{ran},i}) \right)^2 + \left(\frac{\partial \lambda_0}{\partial s_{\text{ran},i}} u_{\text{rel}}(s_{\text{ran},i}) \right)^2 \right] + u^2(\lambda_{\text{sys}}) . \qquad (122)$$

The sensitivity coefficients for σ are:

$$\frac{\partial \sigma}{\partial \lambda_{\text{ran},i}} = \frac{Kc_1}{4\sigma H} \begin{cases} 2s_1(\lambda_1 - \lambda_0)\delta\lambda_1 - s_1\left[(\lambda_1 - \lambda_0)^2 - \sigma^2\right] - s_2\left[(\lambda_2 - \lambda_0)^2 - \sigma^2\right] & \text{if } i = 1 \\ 2s_i(\lambda_i - \lambda_0)\delta\lambda_i + s_{i-1}\left[(\lambda_{i-1} - \lambda_0)^2 - \sigma^2\right] - s_{i+1}\left[(\lambda_{i+1} - \lambda_0)^2 - \sigma^2\right] & \text{if } 1 < i < N \\ 2s_N(\lambda_N - \lambda_0)\delta\lambda_N + s_{N-1}\left[(\lambda_{N-1} - \lambda_0)^2 - \sigma^2\right] + s_N\left[(\lambda_N - \lambda_0)^2 - \sigma^2\right] & \text{if } i = N, \end{cases} \qquad (123)$$

$$\frac{\partial \sigma}{\partial \lambda_{\text{sys}}} = 0, \tag{124}$$

$$\frac{\partial \sigma}{\partial s_{\text{ran},i}} = \frac{s_i \delta \lambda_i K c_1}{4 \sigma H} \left[(\lambda_i - \lambda_0)^2 - \sigma^2 \right], \tag{125}$$

and

$$\frac{\partial \sigma}{\partial s_{\text{sys}}} = 0. \tag{126}$$

Again, $\partial \sigma / \partial \lambda_{\text{ran},i}$ and $\partial \sigma / \partial s_{\text{ran},i}$ are independent of K and c_1 since $K c_1 / H$ is equal to the inverse of the area under the spectral responsivity curve. The uncertainty $u(\sigma)$ is obtained from:

$$u^2(\sigma) = \sum_{i=1}^{N} \left[\left(\frac{\partial \sigma}{\partial \lambda_{\text{ran},i}} u(\lambda_{\text{ran},i}) \right)^2 + \left(\frac{\partial \sigma}{\partial s_{\text{ran},i}} u_{\text{rel}}(s_{\text{ran},i}) \right)^2 \right]. \tag{127}$$

Finally, because H, λ_0, and σ are all calculated from the same (λ_i, s_i) data, their uncertainties will be correlated. For any two of these quantities, X_1 and X_2, the covariance is:

$$u(X_1, X_2) = \sum_{i=1}^{N} \frac{\partial X_1}{\partial \lambda_{\text{ran},i}} \frac{\partial X_2}{\partial \lambda_{\text{ran},i}} u^2(\lambda_{\text{ran},i}) + \sum_{i=1}^{N} \frac{\partial X_1}{\partial s_{\text{ran},i}} \frac{\partial X_2}{\partial s_{\text{ran},i}} u_{\text{rel}}^2(s_{\text{ran},i})$$
$$+ \frac{\partial X_1}{\partial \lambda_{\text{sys}}} \frac{\partial X_2}{\partial \lambda_{\text{sys}}} u^2(\lambda_{\text{sys}}) + \frac{\partial X_1}{\partial s_{\text{sys}}} \frac{\partial X_2}{\partial s_{\text{sys}}} u_{\text{rel}}^2(s_{\text{sys}}). \tag{128}$$

Thus

$$u(H, \lambda_0) = \sum_{i=1}^{N} \left[\frac{\partial H}{\partial \lambda_{\text{ran},i}} \frac{\partial \lambda_0}{\partial \lambda_{\text{ran},i}} u^2(\lambda_{\text{ran},i}) + \frac{\partial H}{\partial s_{\text{ran},i}} \frac{\partial \lambda_0}{\partial s_{\text{ran},i}} u_{\text{rel}}^2(s_{\text{ran},i}) \right], \tag{129}$$

$$u(H, \sigma) = \sum_{i=1}^{N} \left[\frac{\partial H}{\partial \lambda_{\text{ran},i}} \frac{\partial \sigma}{\partial \lambda_{\text{ran},i}} u^2(\lambda_{\text{ran},i}) + \frac{\partial H}{\partial s_{\text{ran},i}} \frac{\partial \sigma}{\partial s_{\text{ran},i}} u_{\text{rel}}^2(s_{\text{ran},i}) \right], \tag{130}$$

and

$$u(\lambda_0, \sigma) = \sum_{i=1}^{N} \left[\frac{\partial \lambda_0}{\partial \lambda_{\text{ran},i}} \frac{\partial \sigma}{\partial \lambda_{\text{ran},i}} u^2(\lambda_{\text{ran},i}) + \frac{\partial \lambda_0}{\partial s_{\text{ran},i}} \frac{\partial \sigma}{\partial s_{\text{ran},i}} u_{\text{rel}}^2(s_{\text{ran},i}) \right]. \tag{131}$$

These correlated components should be added to Eq. (111) when calculating the total uncertainty in the value of T. The additional terms to be added to $u^2(T)$ are:

$$2 \left[\frac{\partial T}{\partial H} \frac{\partial T}{\partial \lambda_0} u(H, \lambda_0) + \frac{\partial T}{\partial H} \frac{\partial T}{\partial \sigma} u(H, \sigma) + \frac{\partial T}{\partial \lambda_0} \frac{\partial T}{\partial \sigma} u(\lambda_0, \sigma) \right]. \tag{132}$$

However, in practice, these terms are generally negligible compared to those in Eq. (111) and can be ignored.

Once again, GUM Tree Calculator (GTC), as described in Appendix A.2, can be used to automatically propagate the uncertainties in the (λ_i, s_i) and K measurements through Eqs (101) to (103) to give $u(H)$, $u(\lambda_0)$, and $u(\sigma)$ directly, which can then be used in Eq. (111).

B.2 How to Apply the Method for Different Sources of Uncertainty

This method is applied by calculating the integral quantities of Eqs (101) to (103) and then the sensitivity coefficients in Eqs (104) to (108) and Eq. (110). The appropriate sensitivity coefficients for common sources of uncertainty are calculated as follows.

Effect	Notes	Calculation
Spectral responsivity of trap detector, s_{trap}	If spectral in $s(\lambda)$, which affects the central wavelength and bandwidth.	Contributes to H as a component in K. $\dfrac{\partial T}{\partial H}$ from Eq. (104).
Geometric factor, g	Uncertainty associated with geometric factor given by Eqs (24) and (28). Then in H through K.	$\dfrac{\partial H}{\partial g} = \dfrac{H}{g}$ $\dfrac{\partial T}{\partial H}$ from Eq. (104).
Amplifier gain, G	In H through K.	$\dfrac{\partial H}{\partial G} = \dfrac{H}{G}$ $\dfrac{\partial T}{\partial H}$ from Eq. (104).
Wavelength scale accuracy	This produces an uncertainty assoc. with both λ_0 and σ. However, if the accuracy can be considered a spectral offset, it can be considered a simple uncertainty associated with λ_0 only.	Eqs (105) and (106).
Filter stability	This will affect the shape of $s(\lambda)$ and hence both λ_0 and σ. It is best modelled to estimate an uncertainty associated with those.	Eqs (105) and (106).
Instrument stability and noise	This affects the measured signal, S.	Eq. (110).
Size-of source effect, K_{SSE}	In H through K.	$\dfrac{\partial T}{\partial K_{\text{SSE}}} = \dfrac{\partial H}{\partial K_{\text{SSE}}} \dfrac{\partial T}{\partial H}$ $\dfrac{\partial H}{\partial K_{\text{SSE}}} = \dfrac{H}{K_{\text{SSE}}}$ $\dfrac{\partial T}{\partial H}$ from Eq. (104).

Linearity, K_{lin}	In H through K.	$\dfrac{\partial T}{\partial K_{lin}} = \dfrac{\partial H}{\partial K_{lin}} \dfrac{\partial T}{\partial H}$ $\dfrac{\partial H}{\partial K_{lin}} = \dfrac{H}{K_{lin}}$ $\dfrac{\partial T}{\partial H}$ from Eq. (104).
Blackbody emissivity, ε	In S when measuring a blackbody at an unknown temperature.	$\dfrac{\partial T}{\partial \varepsilon} = \dfrac{\partial S}{\partial \varepsilon} \dfrac{\partial T}{\partial S}$ $\dfrac{\partial S}{\partial \varepsilon} = \dfrac{S}{\varepsilon}$ $\dfrac{\partial T}{\partial S}$ from Eq. (110).
Blackbody stability, ability to define melt and similar	As above.	
Hybrid method: lens transmittance	If spectral in $s(\lambda)$, which affects the central wavelength and bandwidth. But normally in H through K.	$\dfrac{\partial T}{\partial \tau_{abs}} = \dfrac{\partial H}{\partial \tau_{abs}} \dfrac{\partial T}{\partial H}$ $\dfrac{\partial H}{\partial \tau_{abs}} = \dfrac{H}{\tau_{abs}}$ $\dfrac{\partial T}{\partial H}$ from Eq. (104).
Power method: uniformity of detector	These can all be considered as a relative uncertainty in H through K.	$\dfrac{\partial T}{\partial H}$ from Eq. (104).
Radiance method: angular uniformity of the calibration source		
Irradiance/hybrid method: spatial uniformity of the calibration irradiance field		

Note that many sources of uncertainty will be expressed as relative uncertainties rather than absolute uncertainties (with units). All uncertainties in the equations above are absolute uncertainties. However, as an example, consider an amplifier gain. From the table above, this is:

$$\frac{\partial T}{\partial G} = \frac{\partial H}{\partial G} \frac{\partial T}{\partial H} \approx \frac{n \lambda_0 T^2}{G c_2} . \tag{133}$$

Therefore, the uncertainty in temperature due to amplifier gain is

$$
\begin{aligned}
u(T_G) &= \frac{n \lambda_0 T^2}{c_2} \left(\frac{u(G)}{G} \right) \\
&= \frac{n \lambda_0 T^2}{c_2} u_{rel}(G),
\end{aligned}
\tag{134}
$$

where the term $u(G)/G$ is the relative uncertainty in the gain.

References

1. L P Boivin, C Bambera, A A Gaertner, R K Gerson, D J Woods, E R Woolliams, "Wideband filter radiometers for blackbody temperature measurements", *Journal of Modern Optics*, **57**, 1648–1660, 2010.

2. A A Gaertner, "Index of refraction effects in blackbody temperature measurements", 2011; available from: http://www.bipm.org/cc/CCT/Allowed/25/D11_CCTdraftAAG.pdf.

3. V E Anderson, N P Fox, D H Nettleton, "Highly stable, monochromatic and tunable optical radiation source and its application to high accuracy spectrophotometry", *Applied Optics*, **31**, 536–545, 1992.

4. S W Brown, G P Eppeldauer, K R Lykke, "NIST facility for Spectral Irradiance and Radiance Responsivity Calibrations with Uniform Sources", *Metrologia*, **37**, 579–582, 2000.

5. D R Taubert , R Friedrich, J Hartmann, J Hollandt, "Improved calibration of the spectral responsivity of interference filter radiometers in the visible and near infrared spectral range at PTB", *Metrologia*, **40**, S35–S38, 2003.

6. D R Taubert, R Friedrich, J Hartmann, P Sperfeld, J Hollandt, "Long-term stability of the spectral responsivity of filter radiometers at the PTB" in *Proceedings of TEMPMEKO 2004, 9th International Symposium on Temperature and Thermal Measurements in Industry and Science*, edited by D Zvizdic, LPM/FSB, Zagreb, pp. 977–982, 2005.

7. J Reader, "Metrological implications of recent interferometric wavelength measurements for singly ionized silicon in the vacuum ultraviolet (152 nm and 180 nm)", *Metrologia*, **39**, 391–394, 2002.

8. P Saunders, "Uncertainty arising from the use of the mean effective wavelength in realizing ITS-90", in *Temperature: Its Measurement and Control in Science and Industry*, Vol. 7, edited by D C Ripple et al., AIP Conference Proceedings, Melville, New York, 639–644, 2003.

9. JCGM, JCGM 100:2008, *Evaluation of measurement data – Guide to the expression of uncertainty in measurement*, BIPM, 2008.

10. J Hartmann, "High-temperature measurement techniques for the application in photometry, radiometry and thermometry", *Physics Reports*, **469**, 205–269, 2009.

11. http://www.townetech.com/aperture.htm.

12. X Lu, K Anhalt, R D Taubert, Z Yuan, "A comparison of irradiance responsivity and thermodynamic temperature measurement between PTB and NIM", in *Temperature: Its Measurement and Control in Science and Industry*, Vol. 8, edited by C W Meyer, AIP Conference Proceedings, Melville, New York, pp. 728–733, 2013.

13. A D W Todd, D J Woods, "Thermodynamic temperature measurements of the melting temperatures of Co-C, Pt-C and Re-C fixed points at NRC", *Metrologia*, **50**, 20–26, 2013.

14. www.semrock.com.

15. Y S Yoo, G J Kim, S Park, D-H Lee, B-H Kim, "Spectral responsivity calibration of the reference radiation thermometer at KRISS by using a super-continuum laser-based high-accuracy monochromatic source", *Metrologia*, **53**, 1354–1364, 2016.

16. M Lequime, S Liukaityte, M Zerrad, C Amra, "Ultra-wide-range measurements of thin-film filter optical density over the visible and near-infrared spectrum", *Optics Express*, **23**, 26863–26878, 2015.

17. W R Blevin, W J Brown, "A precise measurement of the Stefan-Boltzmann constant", *Metrologia*, **7**, 15–29, 1970.

18. W H Steele, M De, J A Bell, "Diffraction corrections in radiometry", *Journal of the Optical Society of America*, **62**, 1099–1103, 1972.

19. E L Shirley, "Revised formulas for diffraction effects with point and extended sources", *Applied Optics*, **37**, 6581–6590, 1998.

20. L P Boivin, "Measurements using two types of transfer radiometer developed for a monochromator-based cryogenic radiometer facility", *Metrologia*, **35**, 363–368, 1998.

21. N P Fox, J E Martin, D H Nettleton, "Absolute spectral radiometric determination of the thermodynamic temperatures of the melting/freezing points of gold, silver and aluminium", *Metrologia*, **28**, 357–374, 1991.

22. J Hartmann, D R Taubert, J Fischer, "Measurements of $T–T_{90}$ down to Zinc point temperatures with absolute filter radiometry", in *Proceedings of TEMPMEKO 2001, 8th International Symposium on Temperature and Thermal Measurements in Industry and Science*, edited by B Fellmuth, J Seidel, G Scholz, VDE Verlag GmbH, Berlin, pp. 377–382, 2002.

23. J Hartmann, L Werner, "Radiation thermometry towards the triple point of water?" *International Journal of Thermophysics*, **29**, 1052–1065, 2008.

24. J Hollandt, R Friedrich, B Gutschwager, D Taubert, J. Hartmann, "High-accuracy radiation thermometry at the National Metrology Institute of Germany, the PTB", *High Temperatures–High Pressures*, **35/36**, 379–415, 2005.

25. N Noulkow, R D Taubert, P Meindl, J Hollandt, "Infrared filter radiometers for thermodynamic temperature determination below 660 °C", *International Journal of Thermophysics*, **30**, 131–143, 2009.

26. D R Taubert, J Hartmann, J Hollandt, J Fischer, "Investigation of the accuracy of the ITS-90 with reference to thermodynamic temperature in the range from 400 °C up to 600 °C", in *Temperature: Its Measurement and Control in Science and Industry*, Vol. 7, edited by D C Ripple *et al.*, AIP Conference Proceedings, Melville, New York, pp. 7–12, 2003.

27. K Anhalt, "Radiometric measurement of thermodynamic temperatures during the phase transformation of metal-carbon eutectic alloys for a new high temperature scale above 1000 °C", University of Berlin, 2008.

28. K Anhalt, J Hartmann, D Lowe, G Machin, M Sadli, Y Yamada, "Thermodynamic temperature determinations of Co-C, Pd-C, Pt-C and Ru-C eutectic fixed-point cells", *Metrologia*, **43**, S78–S83, 2006.

29. K Anhalt, Y Wang, Y Yamada, J Hartmann, "Large and small aperture fixed-point cells of Cu, Pt-C and Re-C", *International Journal of Thermophysics*, **29**, 969–983, 2008.

30. E R Woolliams, M R Dury, T A Burnitt, P E R Alexander, R Winkler, W S Hartree, S G R Salim, G Machin, "Primary radiometry for the *Mise-en-Pratique* for the definition of the kelvin: the hybrid method", *International Journal of Thermophysics*, **32**, 1–11, 2011.

31. E R Woolliams, D F Pollard, N J Harrison, E Theocharous, N P Fox, "New facility for the high-accuracy measurement of lens transmission", *Metrologia*, **37**, 603–605, 2000.

32. R Winkler, E R Woolliams, W S Hartree, S G R Salim, N P Fox, J R Mountford, M White, S R Montgomery, "Calibration of an absolute radiation thermometer for accurate determination of fixed-point temperatures", *International Journal of Thermophysics*, **28**, 2087–2097, 2007.

33. H W Yoon, D W Allen, R D Saunders, "Methods to reduce the size-of-source effect in radiation thermometers", in *Proceedings of TEMPMEKO 2004, 9th International Symposium on Temperature and Thermal Measurements in Industry and Science*, edited by D Zvizdic, LPM/FSB, Zagreb, 521–526, 2005.

34. H W Yoon, "The realization and the dissemination of thermodynamic temperature scales", *Metrologia*, **43**, S22–S26, 2006.

35. H W Yoon, D W Allen, C E Gibson, M Litorja, R D Saunders, S W Brown, G P Eppeldauer, K R Lykke, "Thermodynamic-temperature determinations of the Ag and Au freezing temperatures using a detector-based radiation thermometer", *Applied Optics*, **46**, 2870–2880, 2007.

36. H W Yoon *et al.*, "Uncertainty analysis and maintenance of the NIST detector-based temperature scale", *Acta Metrologica Sinica*, **29**, 2008.

37. M L Baker, V L Yen, "Effects of the variation of angle of incidence and temperature on infrared filter characteristics", *Applied Optics*, **6**, 1343–1348, 1967.

38. P H Lissberger, "Effective refractive index as a criterion of performance of interference filters", *Journal of the Optical Society of America*, **58**, 1586–90, 1968.

39. J Meaburn, "The stability of interference filters", *Applied Optics*, **5**, 1757–1759, 1966.

40. Sh A Furman, M D Levina, "Effect of moisture on the optical characteristics of narrow band interference filters", *Optics and Spectrosc*opy (USSR), **30**, 404–408, 1971.

41. D R Taubert, R Friedrich, J Hartmann, P Sperfeld, J Hollandt, "Long term stability of the spectral responsivity of filter radiometers at the PTB", in *Proceedings of TEMPMEKO 2004, 9th International Symposium on Temperature and Thermal Measurements in Industry and Science*, edited by D Zvizdic, LPM/FSB, Zagreb, 977–982, 2005, ISBN 953-6313-73-1.

42. W H Turner, "Photoluminescence of color filter glasses", *Applied Optics*, **12**, 480–486, 1973.

43. P Saunders, H Edgar, "On the characterisation and correction of the size-of-source effect in radiation thermometers", *Metrologia*, **46**, 62–74, 2009.

44. G Machin, R Sergienko, "A comparative study of size-of-source effect (SSE) determination techniques", in *Proceedings of TEMPMEKO 2001, 8th International Symposium on Temperature and Thermal Measurements in Industry and Science*, edited by B Fellmuth, J Seidel, G Scholz, VDE Verlag GmbH, Berlin, 155–160, 2002.

45. H W Yoon, D W Allen, R D Saunders, "Methods to reduce the size-of-source effect in radiometers", *Metrologia*, **42**, 89–96, 2005.

46. M R Dury, T C Arneil, G Machin G, T M Goodman, "Size-of-source effect sensitivities in radiometers", *International Journal of Thermophysics*, **35**, 1391–1400**,** 2014.

47. P Saunders, "Correcting radiation thermometry measurements for the size-of-source effect", *International Journal of Thermophysics*, **32**, 1633–1654, 2011.

48. P Bloembergen, "Analytical representations of the size-of-source effect", *Metrologia*, **46**, 534–543, 2009.

49. P Saunders, "Propagation of uncertainty for non-linear calibration equations with an application in radiation thermometry", *Metrologia*, **40**, 93–101, 2003.

50. P Saunders, D R White, "Propagation of uncertainty due to non-linearity in radiation thermometers", *International Journal of Thermophysics*, **28**, 2098–2110, 2007.

51. P Saunders, D R White, H Edgar, "A compact combinatorial device for measurement of non-linearity of radiation detectors", *International Journal of Thermophysics*, **36**, 290–302, 2015.

52. H W Yoon, J J Butler, T C Larason, G P Eppledauer, "Linearity of InGaAs photodiodes", *Metrologia*, **40**, S154–S158, 2003.

53. V I Sapritsky, A V Prokhorov, "Spectral effective emissivities of nonisothermal cavities calculated by the Monte Carlo method", *Applied Optics*, **34**, 5645–5652, 1995.

54. A V Prokhorov, "Monte Carlo Method in Optical Radiometry", *Metrologia*, **35**, 465–471, 1998.

55. J Hartmann, D Taubert, "Assessing blackbody emissivity by Monte Carlo simulation", in *Proceedings of Infrared Sensors and Systems*, pp. 133–138, 2002.

56. B B Khlevnoy, M L Samoylov, I A Grigoryeva, N A Ibragimov, V I Shapoval, A V Puzanov, S A Ogarev, "Development of high-temperature blackbodies and furnaces for radiation thermometry", *International Journal of Thermophysics*, **32**, 1686–1696, 2011.

57. H W Yoon, C E Gibson, J L Gardner, "Spectral radiance comparison of two blackbodies with temperatures determined using absolute detectors and ITS-90 techniques", in *Temperature: Its Measurement and Control in Science and Industry*, Vol. 7, edited by D C Ripple *et al.*, AIP Conference Proceedings, Melville, New York, pp. 601–606, 2003.

58. J Hartmann, J Hollandt, B Khlevnoy, S Morozova, S Ogarev, F Sakuma, "Blackbody and other calibration sources", Chapter 6, in *Radiometric Temperature Measurements, I. Fundamentals. Experimental Methods in the Physical Sciences*, Volume 42, edited by Z M Zhang, B K Tsai, G Machin, Academic Press, USA, pp. 241–295, 2010.

59. B B Khlevnoy, I A Grigoryeva, M L Samoylov, Y Yamada, "Comparison of Re-C fixed-point cells and their T-90 temperatures between NMIJ and VNIIOFI", *International Journal of Thermophysics*, **32**, 1753–1762, 2011.

60. Y Yamada, K Anhalt, M Battuello, P Bloembergen, B Khlevnoy, G Machin, M Matveyev, M Sadli, T Wang, "Construction of high-temperature fixed-point cells for thermodynamic temperature assignment", in *Temperature: Its Measurement and Control in Science and Industry*, Vol. 8, edited by C. W. Meyer, AIP Conference Proceedings, Melville, New York, pp. 335–339, 2013.

61. P Bloembergen, B Khlevnoy, P Jimeno Largo, Y Yamada, "Spectral and total effective emissivity of a high-temperature fixed-point radiator considered in relation to the temperature drop across its back wall", *International Journal of Thermophysics*, **29**, 370–385, 2008.

62. B B Khlevnoy, V R Gavrilov, D A Otryaskin, I A Grigor'eva, M V Solodilov, M L Samoilov, V I Sapritsky, "Measurement of the thermodynamic temperature of high-temperature fixed points", *Measurement Techniques*, **56**, 433–439, 2013.

63. J Hartmann, K Anhalt, D Taubert, J Hollandt, "Absolute radiometry for the MeP-K: the irradiance measurement method", *International Journal of Thermophysics*, **32**, 1707–1718, 2011.

64. P Sperfeld, K-H Raatz, B Nawo, W Moeller, J. Metzdorf, "Spectral-irradiance scale based on radiometric black-body temperature measurements", *Metrologia*, **32**, 435–439, 1995/96.

65. P Sperfeld, J Metzdorf, S Galal Yousef, K D Stock and, W Moeller, "Improvement and extension of the black-body-based spectral irradiance scale", *Metrologia*, **35**, 267–271, 1998.

66. P Sperfeld, J Metzdorf, N J Harrison, N P Fox, B B Khlevnoy, V B Khromchenko, S N Mekhontsev, V I Shapoval, M F Zelener, V I Sapritsky, "Investigation of high-temperature black body BB3200", *Metrologia*, **35**, 419–422, 1998.

67. J Fischer, M Battuello, M Sadli, M Ballico, S N Park, P Saunders, Y Zundong, B C Johnson, E van der Ham, Wang Li, F Sakuma, G Machin, N Fox, S Ugur, M Matveyev, "Uncertainty budgets for realisation of scales by radiation thermometry", CCT working document CCT03-03, Sèvres, France, May 2003.

68. ATodd, D Lowe, K Anhalt, P Bloembergen, B Khlevnoy, M Sadli, N Sasajima, G Machin, "Report from the CCT Task Group for Non-Contact Thermometry HTFP Uncertainties (CCT TG-NCTh-HTFPU)".

69. E R Woolliams, K Anhalt, M Ballico, P Bloembergen, F Bourson, S Briaudeau, J Campos, M G Cox, D del Campo, W Dong, M R Dury, V Gavrilov, I Grigoryeva, M L Hernanz, F Jahan, B Khlevnoy, V Khromchenko, D H Lowe, X Lu, G Machin, J M Mantilla, M J Martin, H C McEvoy, B Rougié, M Sadli, S G R Salim, N Sasajima, D R Taubert, A D W Todd, R Van den Bossche, E van der Ham, T Wang, A Whittam, B Wilthan, D J Woods, J T Woodward, Y Yamada, Y Yamaguchi, H W Yoon, Z Yuan "Thermodynamic temperature assignment to the point of inflection of the melting curve of high-temperature fixed points", *Phil. Trans. R. Soc. A* 374 20150044; 2016; DOI: 10.1098/rsta.2015.0044.

70. E R Woolliams, "Uncertainty analysis for filter radiometry based on the uncertainty associated with integrated quantities", *International Journal of Thermophysics*, **35**, 1353–1365, 2014.

71. E R Woolliams, "Development and evaluation of a high temperature blackbody source for the realisation of NPL's primary spectral irradiance scale" in *Physics*, University of Manchester, 2003.

72. E R Woolliams, N P Fox, M G Cox, P M Harris, N J Harrison, "Final report on CCPR K1-a: spectral irradiance from 250 nm to 2500 nm", *Metrologia*, **43**, 02003, 2006.

73. B D Hall, "Object-oriented software for evaluating measurement uncertainty", *Measurement Science and Technology*, **24**, 055004, 2013.

74. GUM Tree Calculator (GTC) can be downloaded from the MSL website: http://www.measurement.govt.nz/services/specialist-user-groups/measurement-software-toolkit/software-download-request-form.

75. P Saunders, "Uncertainties in the realisation of thermodynamic temperature above the silver point", *International Journal of Thermophysics*, **32**, 26–44, 2011.

76. F Sakuma, S Hattori, "Establishing a practical temperature standard by using a narrow-band radiation thermometer with a silicon detector", in *Temperature: Its Measurement and Control in Science and Industry*, edited by J F Schooley, AIP, New York, pp. 421–427, 1982.

77. P Saunders, D R White, "Interpolation errors for radiation thermometry", *Metrologia*, **41**, 41–46, 2004.

78. P Saunders, D R White, "Physical basis of interpolation equations for radiation thermometry", *Metrologia*, **40**, 195–203, 2003.